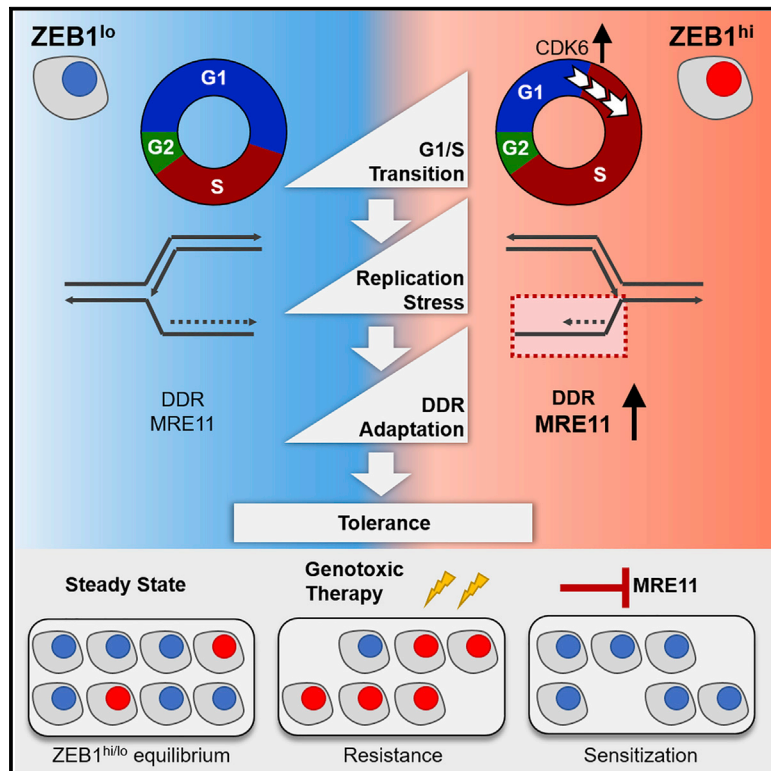


## The EMT transcription factor ZEB1 governs a fitness-promoting but vulnerable DNA replication stress response

### Graphical abstract



### Authors

Harald Schuhwerk, Julia Kleemann, Pooja Gupta, ..., Marc P. Stemmler, Simone Brabletz, Thomas Brabletz

### Correspondence

harald.schuhwerk@fau.de (H.S.), thomas.brabletz@fau.de (T.B.)

### In brief

ZEB1 is heterogeneously expressed in cancer cells. Characterizing subpopulations with high ZEB1 levels (ZEB1<sup>hi</sup>), Schuhwerk et al. show that ZEB1 induces G1/S transition via CDK6 to launch an adaptive MRE11-involving response promoting chemoresistance. Targeting of ZEB1<sup>hi</sup> cells by MRE11 inhibition allows chemosensitization, reinforcing the translational impact of the EMT-DDR interface.

### Highlights

- Intercellular heterogeneity in ZEB1 levels is a general feature of cancer cells
- ZEB1 promotes G1/S transition via CDK6 to inflict endogenous DNA replication stress
- Replication stress tolerance in ZEB1<sup>hi</sup> cells requires MRE11-engaging DDR adaptation
- DDR buildups render ZEB1<sup>hi</sup> cells chemoresistant but sensitive to MRE11 inhibition



## Article

# The EMT transcription factor ZEB1 governs a fitness-promoting but vulnerable DNA replication stress response

Harald Schuhwerk,<sup>1,10,11,\*</sup> Julia Kleemann,<sup>1,10</sup> Pooja Gupta,<sup>2</sup> Ruthger van Roey,<sup>1</sup> Isabell Armstark,<sup>1</sup> Martina Kreileder,<sup>1</sup> Nora Feldker,<sup>1</sup> Vignesh Ramesh,<sup>3</sup> Yussuf Hajjaj,<sup>1</sup> Kathrin Fuchs,<sup>1</sup> Mousumi Mahapatro,<sup>1</sup> Mojca Hribersek,<sup>1</sup> Marco Volante,<sup>4</sup> Arwin Groenewoud,<sup>5,9</sup> Felix B. Engel,<sup>5,9</sup> Paolo Ceppi,<sup>3</sup> Markus Eckstein,<sup>6,9</sup> Arndt Hartmann,<sup>6,9</sup> Fabian Müller,<sup>7</sup> Torsten Kroll,<sup>8</sup> Marc P. Stemmler,<sup>1</sup> Simone Brabletz,<sup>1</sup> and Thomas Brabletz<sup>1,9,\*</sup>

<sup>1</sup>Department of Experimental Medicine 1, Nikolaus-Fiebiger Center for Molecular Medicine, Friedrich-Alexander University of Erlangen-Nürnberg, Erlangen, Germany

<sup>2</sup>Core Unit for Bioinformatics, Data Integration and Analysis, Center for Medical Information and Communication Technology, University Hospital Erlangen, Erlangen Germany

<sup>3</sup>Department of Biochemistry and Molecular Biology, University of Southern Denmark, Odense M, Denmark

<sup>4</sup>Department of Oncology, University of Turin, Orbassano, Turin, Italy

<sup>5</sup>Experimental Renal and Cardiovascular Research, Department of Nephropathology, Institute of Pathology, Friedrich-Alexander-Universität Erlangen-Nürnberg (FAU), Erlangen, Germany

<sup>6</sup>Institute of Pathology, University Hospital Erlangen, Friedrich-Alexander-University Erlangen-Nürnberg, Erlangen, Germany

<sup>7</sup>Department of Internal Medicine 5, Haematology and Oncology, University Hospital Erlangen, Erlangen Germany

<sup>8</sup>Leibniz Institute on Aging - Fritz-Lipmann Institute (FLI), Jena, Germany

<sup>9</sup>Comprehensive Cancer Center Erlangen-EMN, Erlangen University Hospital, Friedrich-Alexander University Erlangen-Nürnberg, Erlangen, Germany

<sup>10</sup>These authors contributed equally

<sup>11</sup>Lead contact

\*Correspondence: [harald.schuhwerk@fau.de](mailto:harald.schuhwerk@fau.de) (H.S.), [thomas.brabletz@fau.de](mailto:thomas.brabletz@fau.de) (T.B.)

<https://doi.org/10.1016/j.celrep.2022.111819>

## SUMMARY

The DNA damage response (DDR) and epithelial-to-mesenchymal transition (EMT) are two crucial cellular programs in cancer biology. While the DDR orchestrates cell-cycle progression, DNA repair, and cell death, EMT promotes invasiveness, cellular plasticity, and intratumor heterogeneity. Therapeutic targeting of EMT transcription factors, such as ZEB1, remains challenging, but tumor-promoting DDR alterations elicit specific vulnerabilities. Using multi-omics, inhibitors, and high-content microscopy, we discover a chemoresistant ZEB1-high-expressing sub-population (ZEB1<sup>hi</sup>) with co-wired cell-cycle progression and proficient DDR across tumor entities. ZEB1 stimulates accelerated S-phase entry via CDK6, inflicting endogenous DNA replication stress. However, DDR buildups involving constitutive MRE11-dependent fork resection allow homeostatic cycling and enrichment of ZEB1<sup>hi</sup> cells during transforming growth factor  $\beta$  (TGF- $\beta$ )-induced EMT and chemotherapy. Thus, ZEB1 promotes G1/S transition to launch a progressive DDR benefitting stress tolerance, which concurrently manifests a targetable vulnerability in chemoresistant ZEB1<sup>hi</sup> cells. Our study thus highlights the translationally relevant intercept of the DDR and EMT.

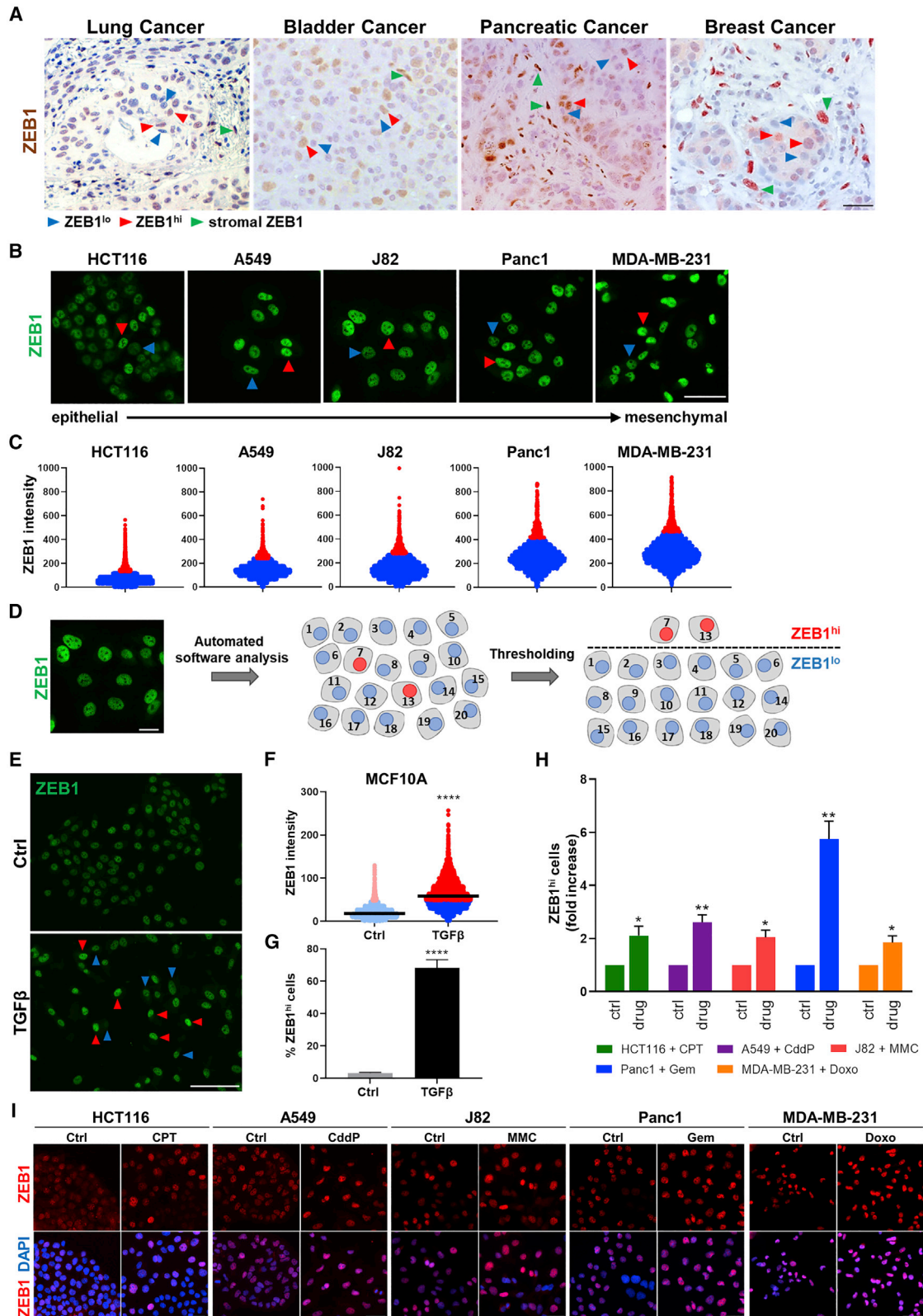
## INTRODUCTION

The DNA damage response (DDR) is a cell-cycle-dependent signaling network orchestrating DNA repair, proliferation, and cell death in response to DNA damages, such as those occurring during DNA replication or chemotherapies. Alterations in the DDR, either as a driver of tumorigenesis or as a way to resist genotoxic therapies, are common in cancers. Thus, the targeting of specific branches of the DDR is emerging as a therapeutic avenue.<sup>1–3</sup> In particular, DNA replication stress is gaining increased attention.<sup>1,4–7</sup> In fact, many synthetic lethal interactions are linked to disturbed DNA replication, for instance,

PARP inhibitors in BRCA1/2- and other homologous recombination (HR)-deficient ovarian and breast cancers, but also other DDR inhibitors.<sup>8–13</sup> These are encouraging prospects as various resistance mechanisms, e.g., drug efflux, bypass of signaling pathways, or cell death evasion,<sup>14</sup> restrict efficient treatment.

Treatment failure in clinics can also arise from genetic, chromatin architectural, transcriptional, and phenotypic heterogeneity in tumor areas and tumor cells within one area.<sup>15,16</sup> This is substantially established by stem-like cancer cells (CSCs) combining high plasticity and the potential to self-renew or differentiate with robustness to various noxae, thereby exerting a devastating impact on treatment success. Accumulating data suggest that





(legend on next page)

CSCs exhibit chemoprotective changes in the DDR and may thus be selectively targeted to prevent disease relapse.<sup>17–22</sup> However, the precise nature and generality of these alterations in CSCs is unclear. Likewise, it is largely unknown to what extent these are pre-existing or acquired during tumor progression or therapy.

Cells with CSC-like features can be generated by epithelial-to-mesenchymal transition (EMT).<sup>23,24</sup> Particularly the EMT-transcription factor (TF) ZEB1 is an established key inducer of cellular plasticity and stemness promoting malignant tumor progression to metastasis.<sup>25–29</sup> Consistently, ZEB1 expression is associated with metastasis and poor prognosis in several cancer types, including colorectal, pancreatic, lung, breast, osteosarcoma, and glioblastoma.<sup>30–34</sup>

EMT activation and resistance to standard therapies appear strongly interconnected.<sup>35–37</sup> EMT-TFs, such as ZEB1, and their associated changes in the chromatin landscape were shown to promote chemo-/radioresistance across several cancer entities.<sup>27,29,34,36,38–40</sup> Studies linked ZEB1-mediated resistance to inhibition of microRNA (miRNA) transcription<sup>34,41</sup> and the DDR kinase ATM,<sup>42,43</sup> but mechanistic insights still appear intricate. Supporting this notion, partially distinct “non-core EMT” functions of EMT-TFs are progressively being discovered,<sup>29,44</sup> as the associated “phenotypic plasticity” cannot be explained by the mere reprogramming toward a mesenchymal phenotype.

Selective targeting of EMT or the DDR to improve chemotherapies are promising approaches, but intercellular heterogeneity and co-dependent pathway shifts are clouding the mechanisms underlying the divergent reactions. This is often sparsely addressed, mainly attributed to high experimental complexity. Here, we studied the intercellular heterogeneity in ZEB1 expression and identified a sub-population of ZEB1-high-expressing (ZEB1<sup>hi</sup>) cells in tumors and in cell cultures that exerts a ZEB1-driven rewiring of cell-cycle progression, inducing an adaptive replication stress response. Although ZEB1<sup>hi</sup> cells benefit from enhanced resistance to DNA damage, they concomitantly become remarkably dependent on the DDR nuclease MRE11 across cancer entities, exposing a potential selective vulnerability of therapy-resistant ZEB1<sup>hi</sup> cells.

## RESULTS

### Intercellular ZEB1 heterogeneity is conserved across different cancer entities

Intratumor heterogeneity due to genetic evolution or cellular plasticity determines tumor progression and clinical responses.

As ZEB1 is a crucial cell plasticity factor, we investigated whether heterogeneity is also reflected in ZEB1 expression on the single-cell level using immunohistochemistry. We observed a strong intercellular heterogeneity in ZEB1 expression in cancer cells of various epithelial tumor types (Figure 1A) with tumor cells containing high amounts of ZEB1 (ZEB1<sup>hi</sup>) next to cells with low amounts (ZEB1<sup>lo</sup>). Immunofluorescence (IF) staining revealed that this pattern was preserved in various cell lines from different tumor entities (Figure 1B). We then scored ZEB1 levels in individual cells by high-content IF, employing a tool for molecular fingerprinting of intracellular signaling events on a single-cell level termed HiMAC.<sup>45,46</sup> As expected, the cell lines contained increasing amounts of ZEB1 along the epithelial (HCT116, A549, J82) to mesenchymal (Panc1, MDA-MB-231) axis (Figures 1B and 1C). However, a small fraction of cells with higher levels than the majority of the population remained between cell lines. Thus, we defined the upper 10% of the cells within each cell line as the ZEB1<sup>hi</sup> sub-population and the residual cells as ZEB1<sup>lo</sup> (Figures 1B–1D). In order to clarify if this heterogeneity in ZEB1 is maintained after EMT, we treated the MCF10A cells with transforming growth factor  $\beta$  (TGF- $\beta$ ) to model EMT (Figures S1A–S1C), which enriched the ZEB1<sup>hi</sup> fraction dramatically, although many ZEB1<sup>lo</sup> cells remained (Figures 1E–1G).

We next reasoned that this heterogeneity in ZEB1 may be modulated during chemotherapy to promote resistance. Therefore, we exposed different cancer cell lines to moderate doses of the respective chemotherapeutics and scored the ZEB1<sup>lo/hi</sup> sub-populations after 72 h. The fraction of ZEB1<sup>hi</sup> cells increased in all lines (Figures 1H and 1I), in fact without robustly elevating the ZEB1 content per cell within each sub-population (Figure S1D). Notably, the TGF- $\beta$ -induced ZEB1<sup>hi</sup> subpopulation of MCF10A cells also increased in response to different DNA damages (Figure S1E). Taken together, these data demonstrate that intercellular heterogeneity in ZEB1 levels is a general phenomenon across cell lines and entities and that the ZEB1<sup>hi</sup> sub-populations, but not necessarily the intracellular ZEB1 level, are enriched after chemotherapy.

### Single-cell transcriptomics reveals changes in cell-cycle progression of ZEB1<sup>hi</sup> cells

To gain insight into the global characteristics of ZEB1<sup>hi</sup> cells, we performed single-cell (sc) transcriptomics (Figure 2A). We selected routinely cultured MDA-MB-231 as model system to maintain comparability with available transcriptomes and chromatin immunoprecipitation sequencing (ChIP-seq) data<sup>31,47</sup> and to avoid the

### Figure 1. Intercellular ZEB1 heterogeneity is conserved across different cancer types

- (A) ZEB1 immunohistochemistry of human tumor sections. Arrowheads mark cells as ZEB1<sup>lo/hi</sup> (blue/red) and stromal (green). Scale bar, 20  $\mu$ m.  
 (B) Representative images of ZEB1 IF of cancer cell lines. Red arrowheads mark ZEB1<sup>hi</sup> cells and blue ones ZEB1<sup>lo</sup> cells. Scale bar, 50  $\mu$ m.  
 (C) Scatterplots depicting ZEB1 signal intensities in cancer cell lines. ZEB1<sup>lo/hi</sup> cells are filled in blue/red.  
 (D) Scheme of the IF analysis of ZEB1 by HiMAC. For details, see STAR Methods. Scale bar, 20  $\mu$ m.  
 (E–G) Analysis of ZEB1 heterogeneity in MCF10A cells after stimulation with TGF- $\beta$  or solvent control (Ctrl) for 10 days.  
 (E) Representative images of ZEB1 IF. Red and blue arrowheads indicate ZEB1<sup>hi</sup> and ZEB1<sup>lo</sup> cells, respectively. Scale bar, 100  $\mu$ m.  
 (F) Scatterplots of ZEB1 IF intensities with the median (horizontal line) showing ZEB1<sup>lo/hi</sup> cells in blue/red.  
 (G and H) Scoring of ZEB1<sup>hi</sup> cells in Ctrl-/TGF- $\beta$ -treated MCF10A cells (G) and in cell lines after 72 h of chemotherapy (H).  
 (I) Representative ZEB1 IF images of cells from (H). Scale bar, 40  $\mu$ m.

Data are depicted as the mean  $\pm$  SEM of  $n \geq 3$  independent experiments (G and H) or of  $\geq 2,000$  individual cells per group (C and F) derived of  $n \geq 3$  independent experiments. Asterisks (\*) mark significance as determined by Mann-Whitney test (F) or Student's t test (G and H) comparing drug treated with the solvent control. \* $p < 0.05$ , \*\* $p < 0.01$ , \*\*\* $p < 0.001$ , \*\*\*\* $p < 0.0001$ .

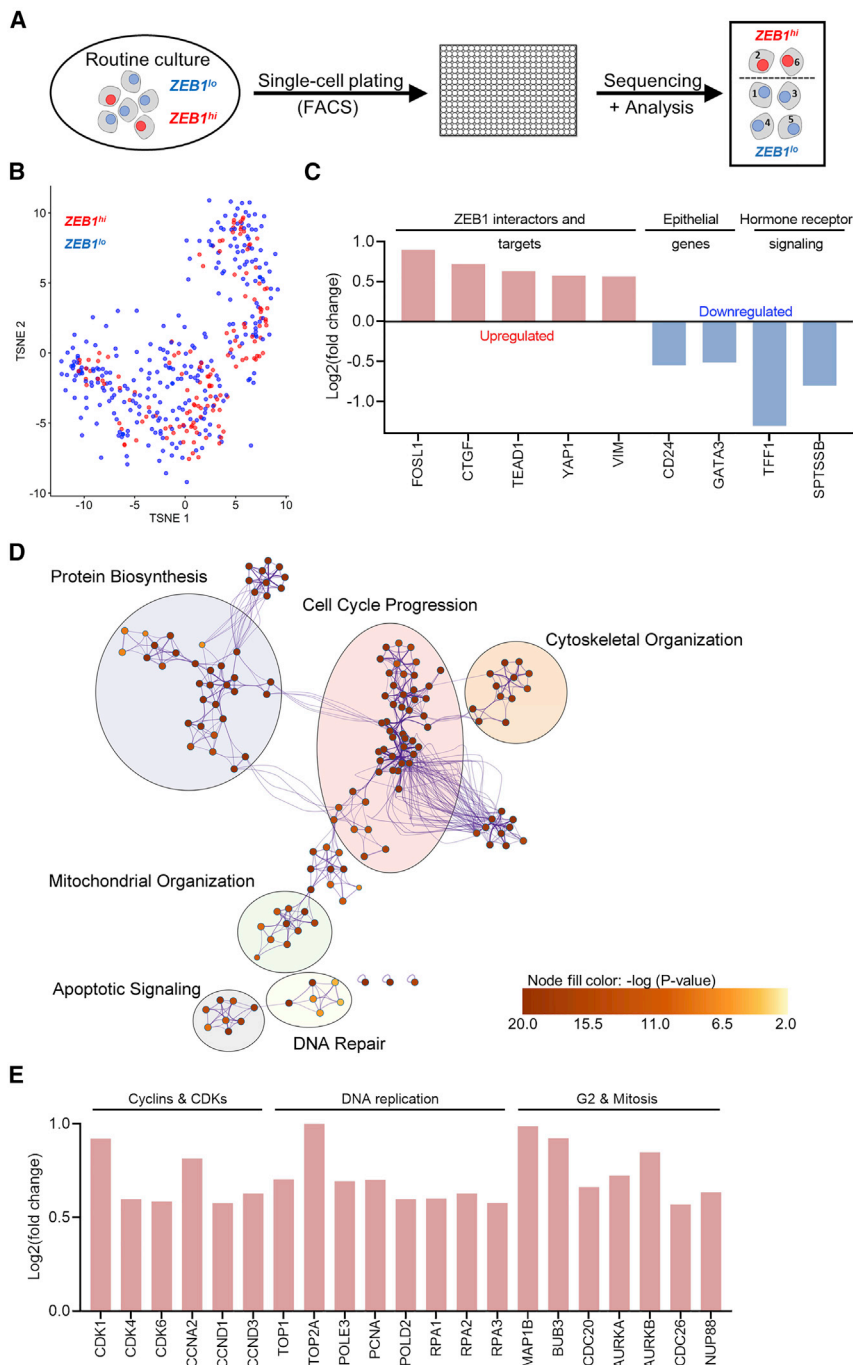


**Figure 2. Single-cell RNA sequencing reveals enrichment of cell-cycle regulators in  $ZEB1^{hi}$  cells**

(A) Scheme of the single-cell sequencing approach of routinely cultured MDA-MB-231 cells.

(B) Distribution of  $ZEB1^{lo}$  and  $ZEB1^{hi}$  cells on t-distributed stochastic neighbor embedding (t-SNE) clusters from scRNA sequencing. Please refer to Figure S2 for clustering and gating strategy.

(C) Differentially expressed genes in  $ZEB1^{hi}$  versus  $ZEB1^{lo}$  cells ( $p < 0.01$ ; false discovery rate [FDR]  $< 0.1$ ).

(D) Metascape analysis showing gene enrichment network in  $ZEB1^{hi}$  cells relative to  $ZEB1^{lo}$  ( $p < 0.01$ ; FDR  $< 0.05$ ). Please refer to Table S2.

(E) Upregulated genes in  $ZEB1^{hi}$  cells as in (C).

$ZEB1^{lo}$  groups, which distributed evenly along the original cell clusters (Figures 2B and S2D). As expected, the  $ZEB1^{hi}$  cells displayed increased expression of *VIM* and known ZEB1 interactors and target genes, such as *YAP* and *FOSL1*,<sup>31</sup> but low levels of the epithelial genes *CD24* and *GATA3* (Figure 2C). Although  $ZEB1^{hi}$  cells showed ample changes in gene expression (Table S1), neither *ZEB2* nor *SNAI1/2* were differentially expressed in the  $ZEB1^{hi}$  cells (Figure S2D), implying distinct functions of EMT-TFs in unchallenged MDA-MB-231. When comparing the transcriptomes of  $ZEB1^{hi}$  and  $ZEB1^{lo}$  cells, we obtained profound enrichment of terms associated with cell-cycle progression in  $ZEB1^{hi}$  cells alongside biosynthetic terms (Figure 2D; Table S2). Specifically, they displayed elevated levels of several cyclin-dependent kinases, cyclins, replicative polymerases, topoisomerases, replication protein A, and mitotic genes (Figure 2E). Supporting the differential expression of S-G2 phase and mitotic genes in  $ZEB1^{hi}$  cells in a pre-clinical *in vivo* setting, the same strategy employed on a patient-derived xenograft (PDX) sc transcriptome dataset before gene set enrichment analysis (GSEA) revealed a significant enrichment in the “G2/M checkpoint hallmark” in  $ZEB1^{hi}$  cells (Figure S2E). As the transcriptional differences of  $ZEB1^{hi}$  cells had no apparent effect on proliferation in

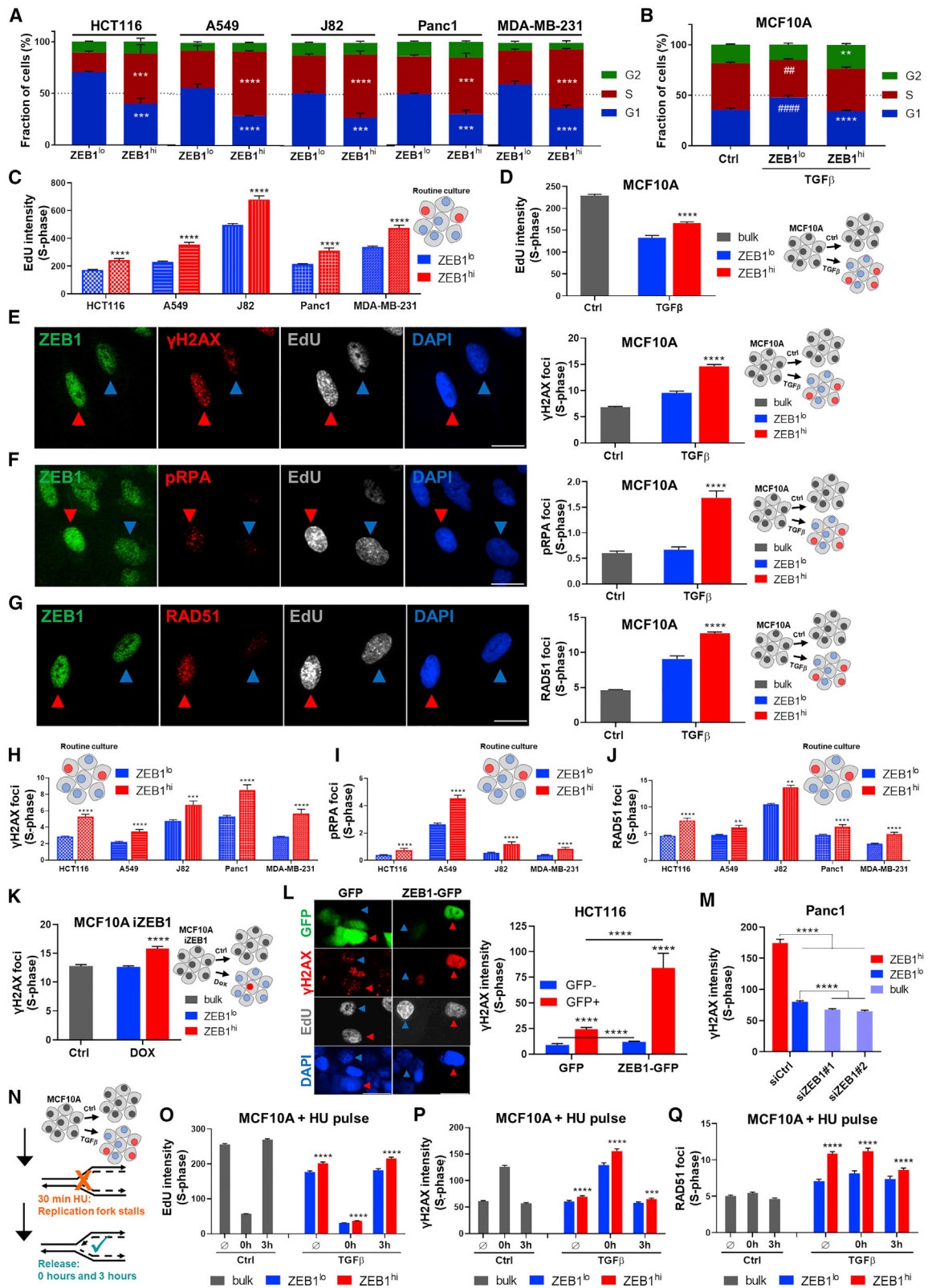
culture, these data altogether suggest that  $ZEB1^{hi}$  cells exhibit cell-cycle changes that do not stimulate cell production under routine culture conditions.

pleiotropic effects of TGF- $\beta$ . We observed four distinct clusters (Figure S2A), indicating heterogeneity in gene expression within one cell line. *ZEB1* was robustly expressed throughout the clusters (Figure S2B). Regarding the other major EMT-TFs, we observed a constant expression pattern of *ZEB2* and *SNAI2*, while *SNAI1* was generally poorly expressed (Figure S2B), and *TWIST1/2* were not detected. We then segregated  $ZEB1^{hi}$  and  $ZEB1^{lo}$  cells based on *ZEB1* transcript counts (Figure S2C) to generate  $ZEB1^{hi}$  and

culture, these data altogether suggest that  $ZEB1^{hi}$  cells exhibit cell-cycle changes that do not stimulate cell production under routine culture conditions.

### ZEB1 induces DNA replication stress

We next sought to validate the cell-cycle changes in asynchronously growing  $ZEB1^{hi}$  cancer cells and in *de novo* TGF- $\beta$ -generated  $ZEB1^{hi}$  MCF10A cells by employing HiMAC. We detected



(legend on next page)

an increased fraction of ZEB1<sup>hi</sup> cells in S phase compared with ZEB1<sup>lo</sup> cells across entities during routine culture (Figure 3A) and TGF- $\beta$ -induced EMT (Figure 3B). Notably, TGF- $\beta$ -treated MCF10A cells generally incorporated less EdU during the pulse-labeling than vehicle-treated cells, confirming the expected lowering of replication by TGF- $\beta$ .<sup>48</sup> Intriguingly, ZEB1<sup>hi</sup> S-phase cells in all models displayed more EdU incorporation than ZEB1<sup>lo</sup> cells, indicative of an increased DNA replication rate (Figures 3C and 3D), concomitant to higher  $\gamma$ H2AX as well as pRPA and RAD51 foci in S phase (Figures 3E–3J), marking stronger DDR activation and single-stranded overhangs, respectively. Altogether, these features represent replication stress that is likely accompanied by recombination intermediates.<sup>6,45</sup> As this did not induce 53BP1 foci in any cell-cycle phase, it seemed not to trigger excessive DNA double-strand breaks (DSBs) and was unlikely due to a repair pathway shift from non-homologous end joining (NHEJ) to HR (Figure S3A). Notably, Snai1<sup>hi</sup> cells gated like ZEB1<sup>hi</sup> cells showed a decrease in S phase and did not exhibit higher replication stress (Figures S3B–S3D). These data show that endogenous replication stress is a general and specific feature of ZEB1<sup>hi</sup> cells. In order to link ZEB1 to this effect, we overexpressed ZEB1 using a doxycycline-inducible construct<sup>47</sup> and via transient transfection. ZEB1 overexpression in all models induced  $\gamma$ H2AX in S phase, while small interfering RNA (siRNA)-mediated knockdown of ZEB1 abolished it (Figures 3K–3M and S3E–S3H). In summary, these data demonstrate that ZEB1 itself triggers DNA replication stress.

The DDR is surveilling DNA replication to counteract replication stress by halting, remodeling, and restarting replication forks and coordinating the firing of origins.<sup>6,49</sup> To test whether replication stress in ZEB1<sup>hi</sup> cells may arise from defects therein, we monitored DNA synthesis and DDR to hydroxyurea (HU), a ribonucleotide reductase inhibitor, inducing replication fork stalls due to nucleotide depletion (Figure 3N). HU pulsing expectedly almost abolished EdU incorporation in MCF10A cells, (Figure 3O, 0 h), demonstrating global stalling of replication. To test whether replication restart is faithfully coordinated to avoid detrimental DSBs,<sup>6,50</sup> we released the HU-pulsed cells for 3 h into drug-free medium, allowing complete recovery of DNA synthesis (Figure 3O, 3 h). The time course of DNA synthesis was paralleled by the induction and resolution of S-phase  $\gamma$ H2AX, demonstrating transient DDR activation (Figures 3O and 3P, 0 versus 3 h). Of note, HU treatment did not

induce RAD51 or 53BP1 foci in S phase (Figures 3Q and S3I), indicating an absence of excessive replication fork collapses. Interestingly, DNA replication rates and  $\gamma$ H2AX (and RAD51) levels remained stably elevated upon HU pulsing and recovery in ZEB1<sup>hi</sup> cells compared with their ZEB1<sup>lo</sup> counterparts (Figures 3O–3Q and S3J–S3M), suggesting safe handling of replication forks in ZEB1<sup>hi</sup> cells. Consistently, MDA-MB-231 ZEB1<sup>hi</sup> cells displayed increased expression of several important DDR factors (Figure S3N). Taken together, these data show S-phase DDR proficiency of ZEB1<sup>hi</sup> cells and suggest that apparent DDR defects are not causing their replication stress.

### ZEB1 promotes G1/S transition via CDK6

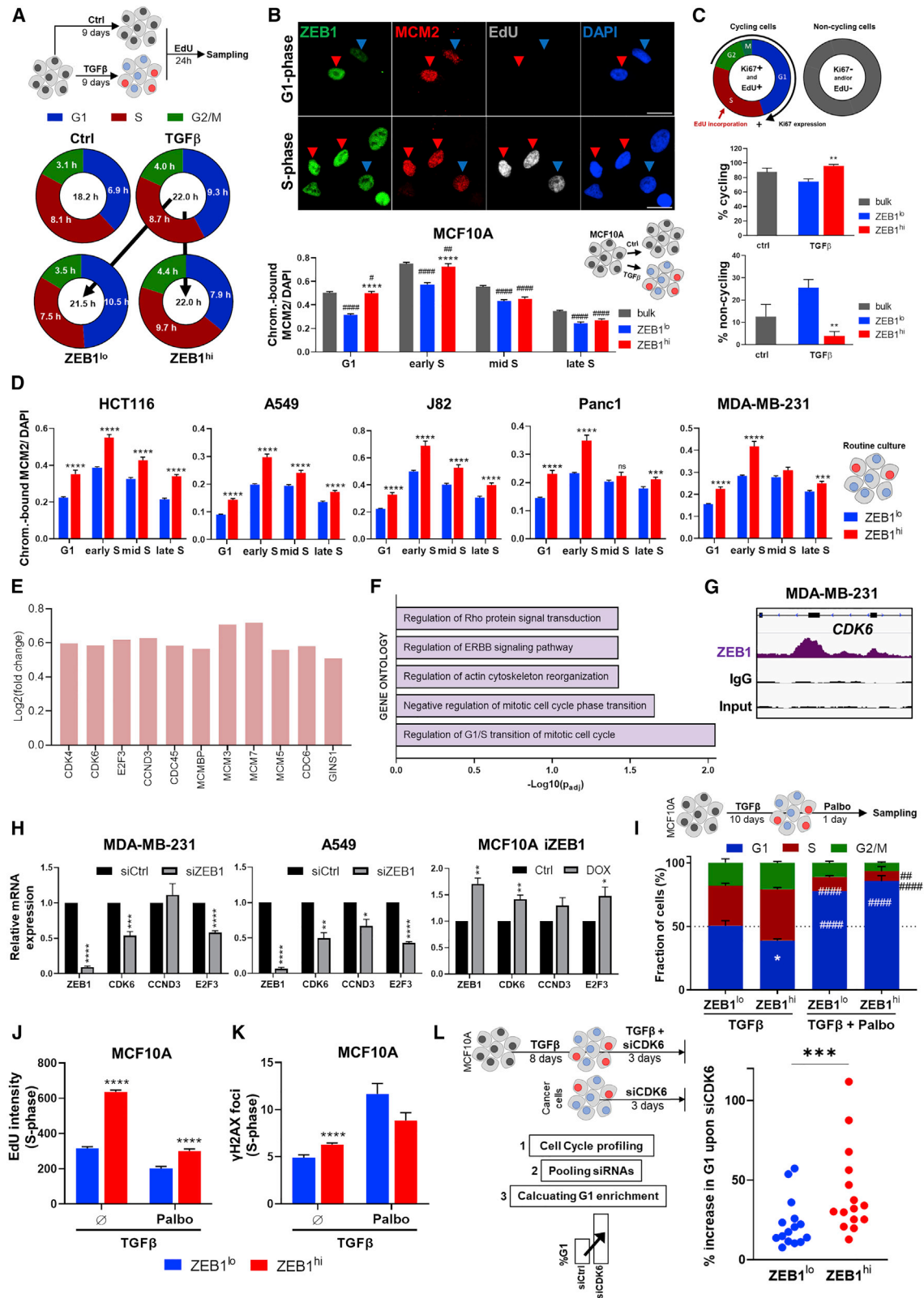
DNA replication stress can be caused by accelerated entry into S phase.<sup>51,52</sup> In order to test whether this occurs in ZEB1<sup>hi</sup> cells, we measured cell-cycle length by cumulative EdU labeling<sup>46</sup> in TGF- $\beta$ -treated MCF10A cells. As expected, TGF- $\beta$  generally prolonged the cell cycle compared with vehicle control (Figures 4A and S4A). Interestingly, ZEB1<sup>lo</sup> and ZEB1<sup>hi</sup> cells both exerted a similar overall lengthening of the cell cycle. While this was almost exclusively due to a huge delay of passing through G1 phase in ZEB1<sup>lo</sup> cells, ZEB1<sup>hi</sup> cells displayed only a moderate increase in G1 length compared with vehicle-treated cells and, consequently, a marked shortening of G1 phase compared with ZEB1<sup>lo</sup> cells (Figures 4A and S4A). The prolonged S phase in ZEB1<sup>hi</sup> cells is consistent with their replication stress (Figures 3D–3G).

Next, we analyzed the loading of minichromosome maintenance complex (MCM) member MCM2 onto chromatin to mark the replicative helicase complex assembled for initiating DNA synthesis. As expected, chromatin-bound MCM2 started in G1 phase, peaked in early S phase, and decreased gradually during S-phase progression (Figure S4B). ZEB1<sup>hi</sup> cells in all models displayed increased loading of MCM2 in early S phase and in G1 phase (Figures 4B and 4D), where the earliest origins are licensed, implying faster commitment to S phase by ZEB1. Consistently, ZEB1 protein levels peaked in early S phase (Figure S4D). Notably, general ZEB1 protein content showed no major fluctuation throughout cell-cycle progression, as deduced from western blotting of ZEB1 from G1-, S-, and G2/M-phase cells separated by fluorescence-activated cell

### Figure 3. ZEB1 induces replication stress without compromising the safe handling of replication forks

(A and B) Cell-cycle profiles of ZEB1<sup>hi</sup> and ZEB1<sup>lo</sup> cells of cancer cell lines (A) and of Ctrl-/TGF- $\beta$ -treated MCF10A cells (B). (C and D) EdU incorporation of indicated cancer cells (C) and of MCF10A Ctrl- and TGF- $\beta$ -induced ZEB1<sup>hi</sup> and ZEB1<sup>lo</sup> cells (D). (E–G) HiMAC of  $\gamma$ H2AX (E), pRPA (F), and RAD51 (G) in MCF10A Ctrl- and TGF- $\beta$ -induced ZEB1<sup>hi</sup> and ZEB1<sup>lo</sup> cells with representative images (left) and quantification (right). Red arrowheads indicate ZEB1<sup>hi</sup> cells and blue ones ZEB1<sup>lo</sup> cells. Scale bar, 20  $\mu$ m. (H–J) Scoring of  $\gamma$ H2AX (H), pRPA (I), and RAD51 foci (J) in cancer cells. (K) Scoring of  $\gamma$ H2AX in MCF10A iZEB1 cells after 72 h Ctrl or doxycycline (Dox) treatment. (L) Representative IF images of  $\gamma$ H2AX and EdU in ZEB1-GFP or GFP-overexpressing HCT116 cells with red and blue arrowheads marking GFP-positive and -negative cells, respectively. Scale bar, 20  $\mu$ m. HiMAC of  $\gamma$ H2AX intensity following GFP or ZEB1-GFP overexpression for 72 h. (M) HiMAC of  $\gamma$ H2AX intensity after 72 h of the indicated siRNA knockdown. (N) Workflow of HU treatment. Ctrl-/TGF- $\beta$ -stimulated cells were treated with HU for 30 min and either fixed directly or after 3 h of recovery in drug-free medium. (O–Q) EdU incorporation (O),  $\gamma$ H2AX intensity (P), and RAD51 foci (Q) of MCF10A Ctrl- and TGF- $\beta$ -induced ZEB1<sup>hi</sup> and ZEB1<sup>lo</sup> cells after treatment according to (N).

Data are depicted as the mean  $\pm$  SEM of  $n \geq 3$  independent experiments (A and B) or the means  $\pm$  SEM of  $\geq 180$  (C),  $\geq 280$  (D–G),  $\geq 150$  (H–J),  $\geq 700$  (K),  $\geq 400$  (L and M), and  $\geq 300$  (O–Q) cells per group of  $n = 3$  independent experiments (C–I, K, M–O) or  $n \geq 2$  (J and L). Indicators (\*/#) mark significance as determined by two-way ANOVA with Sidak's post-test (A and B) comparing ZEB1<sup>lo</sup> with ZEB1<sup>hi</sup> cells (\*) within each cell line or with Ctrl (#) and Mann-Whitney tests (C–Q) comparing ZEB1<sup>hi</sup> with ZEB1<sup>lo</sup> cells, GFP-negative with GFP-positive cells (L), or ZEB1<sup>hi</sup> and ZEB1<sup>lo</sup> with bulk (M). \* $p < 0.05$ , \*\* $p < 0.01$ , \*\*\* $p < 0.001$ , \*\*\*\* $p < 0.0001$ .



(legend on next page)

sorting according to the fluorescent cell-cycle reporter PIP-Fucci<sup>53</sup> (Figure S4C). EdU incorporation in S phase was decreased upon inducible knockdown of *ZEB1*, directly linking full DNA replication rate to *ZEB1* (Figure S4E). Remarkably, only *ZEB1*<sup>lo</sup>, but not *ZEB1*<sup>hi</sup>, cells lowered MCM2 loading at the G1/S border upon TGF- $\beta$  treatment (Figure 4B) and stopped cycling (Figure 4C). These findings indicate that increased initiation of DNA synthesis allows *ZEB1*<sup>hi</sup> cells to escape the anti-proliferative effect of TGF- $\beta$ <sup>48,54</sup> and show that *ZEB1*<sup>hi</sup> cells accelerate G1/S transition.

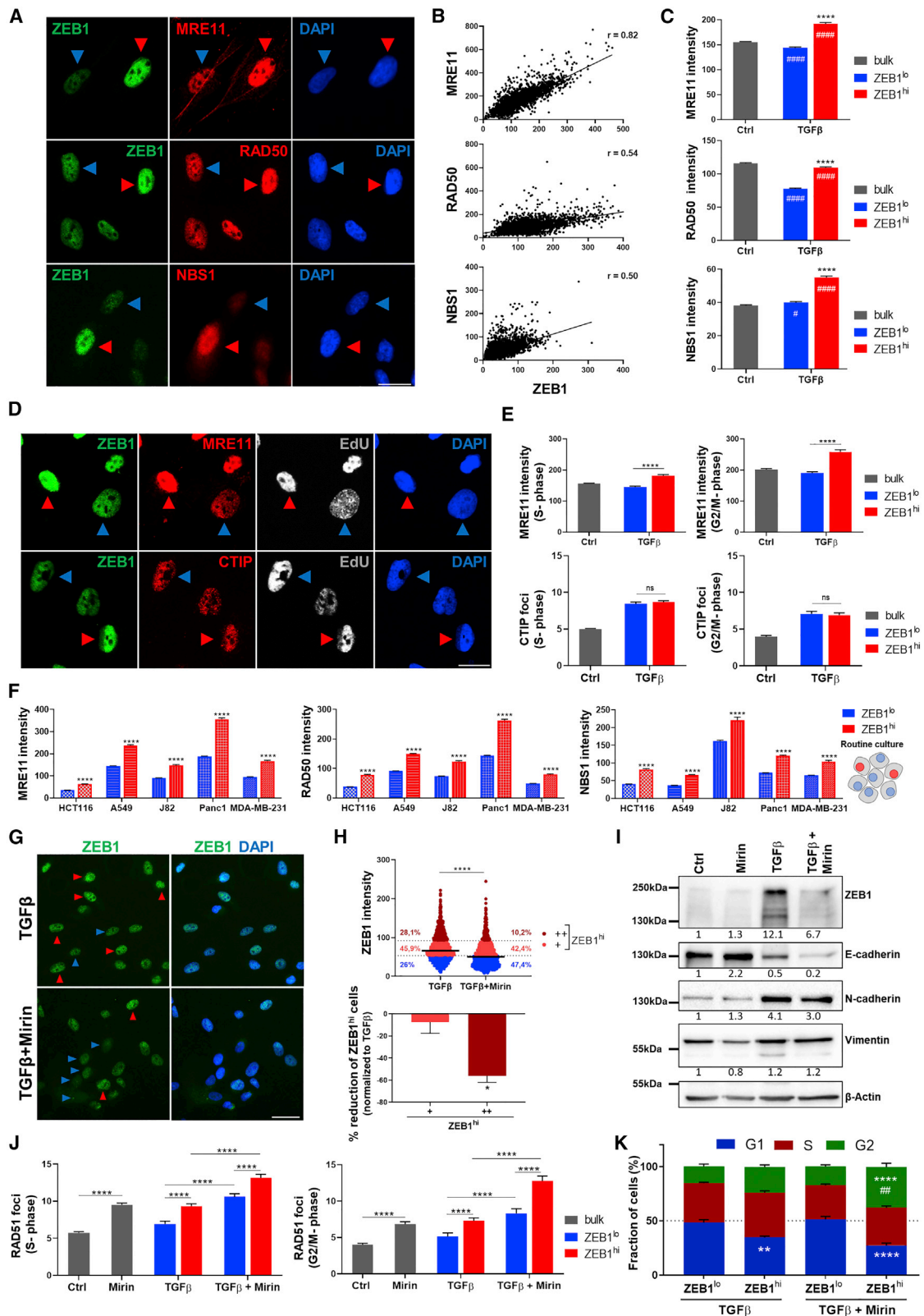
In line with this, Metascape analysis of the MDA-MB-231 *ZEB1*<sup>hi</sup> genes from scRNA-seq revealed terms on G1/S transition ( $\log_{10}(q \text{ value}) \leq -10$ ; Table S2) with upregulation of its key drivers *CDK4*, *CDK6*, and *Cyclin D1/3* (*CCND1/3*), as well as *E2F3* and replication initiation factors (*CDC45*, *MCM7/3*, *CDC6*) (Figure 4E). We then pinpointed activated candidate target genes of *ZEB1*, whose promoters are bound by *ZEB1*, by integrating the *ZEB1*<sup>hi</sup> gene set with *ZEB1*-ChIP-seq and bulk transcriptomes of short hairpin (sh) control (shCtrl) and sh*ZEB1* cells.<sup>31</sup> The shared candidate targets supported altered G1/S transition (Figure 4F; Table S3) and included *CDK6* (Figure 4G), *CCND3*, and *E2F3*. Among these, *CDK6* showed reduced expression upon transient and stable *ZEB1* knockdown across cell lines (Figures 4H and S4F) and was upregulated upon inducible *ZEB1* overexpression (Figure 4H). Publicly deposited *ZEB1* ChIP-seq data ruled out cell-line specificity of *CDK6* as a *ZEB1* candidate target (Figures S4G and S4H). Importantly, short-term treatment with the *CDK4/6* inhibitor palbociclib equalized the rewired cell cycle and diminished the elevated replication stress response in *ZEB1*<sup>hi</sup> cells (Figures 4I–4K). Likewise, siRNA-mediated knockdown of *CDK6* led to a significantly stronger G1-phase enrichment in *ZEB1*<sup>hi</sup> cells, demonstrating their enhanced dependence on *CDK6* for S-phase entry compared with *ZEB1*<sup>lo</sup> cells (Figure 4L). Consequently, *ZEB1*<sup>hi</sup> and *ZEB1*<sup>lo</sup> cells that proceeded to S phase in the absence of *CDK6* showed equalized RAD51 foci (Figures S4J and S4K). Taken together, these data show that *ZEB1* promotes S-phase entry via *CDK6*.

### MRE11-engaging DDR adaptation restrains replication stress in *ZEB1*<sup>hi</sup> cells

As *ZEB1*<sup>hi</sup> cells persisted during routine culture, the DDR in *ZEB1*<sup>hi</sup> cells may have to be co-adapted to tolerate *ZEB1*-induced replication stress. The increase in RAD51 foci in *ZEB1*<sup>hi</sup> cells (Figures 3G and 3J) suggested replication intermediates, resolution of which requires the MRE11-RAD50-NBS1 (MRN) complex.<sup>45,55</sup> Analysis of MRN complex members in TGF- $\beta$ -treated MCF10A cells revealed correlation with *ZEB1* (Figures 5A and 5B). Intriguingly, only TGF- $\beta$ -induced *ZEB1*<sup>hi</sup>, but not *ZEB1*<sup>lo</sup>, cells contained more MRE11 and NBS1 when compared with vehicle-treated cells (Figure 5C). Highlighting MRE11 specificity, CTIP, another S-/G2-/M-phase DDR nuclease, was unchanged (Figures 5D and 5E and S5A). Importantly, we detected MRN enrichment in *ZEB1*<sup>hi</sup> cancer cells compared with *ZEB1*<sup>lo</sup> (Figure 5F), correlation of MRE11 and *ZEB1* in bulk analyses (Figures S5B–S5D), and reproducibly reduced protein levels of MRE11 and RAD50, but not NBS1, upon *ZEB1* knockdown compared with shGFP control lines (Figure S5E). We noticed *ZEB1* binding at the promoters of *MRE11* (*MRE11A*) and *RAD50*, but not *NBS1* (*NBN*), in ChIP-seq<sup>31</sup> and upregulation of MRE11 in *ZEB1*<sup>hi</sup> cells in scRNA-seq (Figure S5F and S3N). Collectively, these data demonstrate that *ZEB1*<sup>hi</sup> cancer cells show a specific upregulation of MRE11, which can be induced by TGF- $\beta$  treatment in non-tumorigenic MCF10A cells. As this may reflect an essential adaptation of *ZEB1*<sup>hi</sup> cells to the *ZEB1*-induced replication stress, we treated MCF10A cells with TGF- $\beta$  and the specific MRE11 inhibitor mirin. Strikingly, mirin strongly reduced the accumulation of *ZEB1*<sup>hi</sup> cells upon TGF- $\beta$ , which was mostly attributable to a decrease in cells with very high levels of *ZEB1* (Figures 5G and 5H). Intriguingly, mirin did not impair mesenchymal morphology or marker expression, such as N-cadherin, vimentin, and loss of E-cadherin (Figure 5I), indicating that a minor upregulation of *ZEB1*, such as in *ZEB1*<sup>lo</sup> cells, may be sufficient to drive classical EMT but not to trigger MRE11-activating replication stress. We then sought to clarify the fate of *ZEB1*<sup>hi</sup> cells in response to mirin. As we did not observe apparent cell death in culture, we hypothesized that unresolved recombination intermediates may cause

### Figure 4. *ZEB1* promotes G1/S transition via *CDK6* causing a replication stress response

(A) Lengths of cell-cycle phases in MCF10A Ctrl- and TGF- $\beta$ -induced *ZEB1*<sup>hi</sup> and *ZEB1*<sup>lo</sup> cells.  
 (B) HiMAC of chromatin-bound MCM2 of MCF10A Ctrl- and TGF- $\beta$ -induced *ZEB1*<sup>hi</sup> and *ZEB1*<sup>lo</sup> cells with representative images (top) and quantification (bottom). Red arrowheads indicate *ZEB1*<sup>hi</sup> cells and blue ones *ZEB1*<sup>lo</sup> cells. Scale bar, 20  $\mu$ m.  
 (C) Determination of cycling activity in MCF10A Ctrl- and TGF- $\beta$ -induced *ZEB1*<sup>hi</sup> and *ZEB1*<sup>lo</sup> cells after 24 h EdU labeling and Ki67 IF by HiMAC.  
 (D) HiMAC of chromatin-bound MCM2 of *ZEB1*<sup>hi</sup> and *ZEB1*<sup>lo</sup> cells in untreated cancer cells.  
 (E) Differential expression of genes related to S-phase entry in MDA-MB-231 *ZEB1*<sup>hi</sup> cells relative to *ZEB1*<sup>lo</sup> cells from single-cell RNA sequencing (scRNA-seq) ( $p < 0.01$ ; FDR  $< 0.1$ ).  
 (F) GSEA using EnrichR of a shared set of genes previously described to be activated by *ZEB1* and those upregulated in *ZEB1*<sup>hi</sup> from scRNA-seq.  
 (G) Integrative Genomics Viewer (IGV) image showing *ZEB1* peaks at the promoter region of *CDK6* from anti-*ZEB1* ChIP-seq.<sup>31</sup>  
 (H) Relative mRNA expression levels (qRT-PCR) of the indicated genes following siRNA-mediated *ZEB1* knockdown or Dox-induced *ZEB1* overexpression for 72 h.  
 (I) Cell-cycle profile of TGF- $\beta$ -treated MCF10A cells  $\pm$  palbociclib (Palbo) treatment for 24 h.  
 (J and K) HiMAC of EdU (J) and  $\gamma$ H2AX foci (K) of TGF- $\beta$ -induced MCF10A *ZEB1*<sup>hi</sup> and *ZEB1*<sup>lo</sup> cells  $\pm$  Palbo.  
 (L) Increase of G1 fraction in *ZEB1*<sup>hi</sup> and *ZEB1*<sup>lo</sup> cells following si*CDK6* knockdown for 72 h in MCF10A + TGF- $\beta$ , MDA-MB-231, A549, and HCT116 cells. The mean of two individual si*CDK6* oligonucleotides is shown.  
 Data are depicted as the mean  $\pm$  SEM of  $n \geq 3$  independent experiments (A, C, H, and I), as data points of  $n \geq 3$  independent experiments of 4 cell lines (L), or the means  $\pm$  SEM of  $>140$  cells (B),  $>100$  HCT116, A549,  $\geq 75$  Panc1, MDA-MB-231,  $>50$  J82 cells (D), or  $\geq 170$  cells (J and K) per group of  $n = 3$  independent experiments. Indicators (\*/#) mark significance as determined by Mann-Whitney tests comparing Ctrl with *ZEB1*<sup>lo/hi</sup> (# in B) or *ZEB1*<sup>lo</sup> with *ZEB1*<sup>hi</sup> (\* in B–D, J, and K); by Student's t test comparing siCtrl with si*ZEB1* or Ctrl with Dox (H); by two-way ANOVA with Sidak's post-test (I) comparing *ZEB1*<sup>hi</sup> with *ZEB1*<sup>lo</sup> (\*) and TGF- $\beta$  + Palbo with TGF- $\beta$  (#); and by paired t test comparing *ZEB1*<sup>lo</sup> with *ZEB1*<sup>hi</sup> (L). \* $p < 0.05$ , \*\* $p < 0.01$ , \*\*\* $p < 0.001$ , \*\*\*\* $p < 0.0001$ .



(legend on next page)

proliferation defects in the mirin-treated ZEB1<sup>hi</sup> cells. Supporting this, mirin treatment increased RAD51 foci strongest in G2-/M-phase of ZEB1<sup>hi</sup> cells (Figure 5J). Consequently, mirin-treated ZEB1<sup>hi</sup> cells exhibited a G2/M arrest (Figure 5K), but the ZEB1<sup>lo</sup> cells remained unaffected. These data are consistent with DNA damage dose-dependent checkpoint activation in S- and G2-/M-phases<sup>56</sup> and shows that TGF- $\beta$ -induced ZEB1<sup>hi</sup>, but not ZEB1<sup>lo</sup>, cells require MRE11 activity for cycling.

### MRE11 inhibition selectively reduces ZEB1<sup>hi</sup> cancer cells and improves chemotherapy

Since accumulation of recombination intermediates in ZEB1<sup>hi</sup> cells was conserved in cancer cell lines, the necessity to resolve them by MRE11 might be a common vulnerability of ZEB1<sup>hi</sup> cells. Therefore, we treated cancer cell lines with mirin (<IC25; Figure S6A) and scored the ZEB1<sup>hi</sup> fraction. Strikingly, mirin treatment reduced all ZEB1<sup>hi</sup> fractions without markedly affecting ZEB1 expression in individual ZEB1<sup>lo/hi</sup> cells (Figures 6A, 6B, and S6B). Based on previously described chemoprotection by ZEB1<sup>27,29,34,36,38–40</sup> and our result that chemotherapy selected for ZEB1<sup>hi</sup> cells (Figures 1H and 1I), we sought to prove chemosensitization by MRE11 inhibition. Based on the regimen in the clinics, we pre-treated the cells with the respective chemotherapeutics before inhibiting MRE11. As expected, chemotherapies reduced cell viability dramatically (by 60%–70%) but also left up to 40% chemoresistant ZEB1<sup>hi</sup>-enriched survivors (Figure S6C, 1H, and 1I). Strikingly, follow-up treatment with mirin and chemotherapy instead of chemotherapy alone further reduced viability in all entities (Figure 6C). Likewise, specific knockdown of *MRE11* or the use of a second MRE11 exonuclease inhibitor (PFM39) decreased cell viability compared with chemotherapy alone (Figures S6D–S6G). These findings strongly suggest that ZEB1<sup>hi</sup> cells can be attacked by mirin for improving chemotherapy. In order to verify this *in vivo*, we xenografted MDA-MB-231 cells with an overall high expression level of ZEB1 and subjected tumor-bearing mice to a treatment regimen applying doxorubicin (Doxo) pulses prior to mirin. Mirin alone did not significantly affect tumor growth (Figures S6H–S6J). While Doxo monotherapy only partially inhibited tumor growth, with a few tumors almost not responding to the therapy at all, the combination therapy with mirin caused complete tumor stasis

(Figures 6D and 6E). These data show that tumors from MDA-MB-231 cells can be sensitized to low-dose Doxo therapy by mirin treatment. Akin to the *in vitro* data, ZEB1<sup>hi</sup> cells enriched in response to Doxo over ZEB1<sup>lo</sup> cells, which was considerably blocked by mirin co-treatment (Figures 6F and 6G). We noted that mirin treatment alone insignificantly reduced the fraction of ZEB1<sup>hi</sup> cells and found a high correlation of ZEB1 and MRE11 expression in all conditions (Figures 6G and 6H). These data demonstrate that ZEB1<sup>hi</sup> cells resist Doxo therapy but are partially sensitive to mirin *in vivo*.

Collectively, these data provide a proof of concept across cancer cell lines and *in vivo* that specific DDR inhibition, as exemplified by MRE11, can improve chemotherapy by selectively targeting the ZEB1<sup>hi</sup> cells.

### DISCUSSION

Here, we discovered a translationally relevant intercellular heterogeneity in the expression of the EMT-TF ZEB1 in tumor tissue and cultured cancer cell lines that is conserved across cancer types. ZEB1<sup>hi</sup> cells display altered expression of cell-cycle regulators, DNA replication, and DDR genes in cultured cell lines and in a published PDX sc transcriptome dataset. ZEB1<sup>hi</sup> cells undergo premature S-phase entry, promoting a DNA replication stress response, which is attributable to activation of the G1/S driver CDK6 and could only be endured due to compensatory upregulation of S/G2/M DDR factors, particularly MRE11 (Figure 6D). This phenotype is specific to ZEB1, as no other EMT-TF was enriched in ZEB1<sup>hi</sup> cells, nor did Snail<sup>hi</sup> cells phenocopy ZEB1<sup>hi</sup> cells. It provided no net benefit for proliferation of ZEB1<sup>hi</sup> cells, which so remained a minor sub-population during routine culture but enriched during chemotherapy *in vitro* and *in vivo*. This is consistent with known ZEB1-linked resistances. Strikingly, MRE11 inhibition reduced the resistant ZEB1<sup>hi</sup> pool, thereby chemosensitizing multiple cancer cell lines and MDA-MB-231 breast tumor xenografts, revealing a potential selective vulnerability of ZEB1<sup>hi</sup> cells in MRE11 activity.

EMT stimuli are often described to be anti-proliferative,<sup>37</sup> but there are conflicting reports on the role of ZEB1 in proliferation. While it was demonstrated that ZEB1 is required for the full replicative potential of mouse embryonic fibroblasts and

### Figure 5. ZEB1<sup>hi</sup> cells engage MRE11 to restrain endogenous replication stress

(A–C) HiMAC of ZEB1 co-stained with MRE11, RAD50, or NBS1 in Ctrl- and TGF- $\beta$ -treated MCF10A cells with representative IF images (A) marking ZEB1<sup>hi</sup> (red arrowheads) and ZEB1<sup>lo</sup> cells (blue arrowheads), scatterplots of the signal intensities with linear regression, and Pearson's r correlation in bulk populations (B) and averaged as bar graphs in Ctrl and ZEB1<sup>lo/hi</sup> cells (C). Scale bar, 20  $\mu$ m.

(D and E) HiMAC of MRE11 and CTIP of MCF10A Ctrl- and TGF- $\beta$ -induced ZEB1<sup>hi</sup> and ZEB1<sup>lo</sup> cells with representative IF images (D) and quantifications (E). Scale bar, 20  $\mu$ m.

(F) HiMAC of the indicated cancer cell lines and proteins.

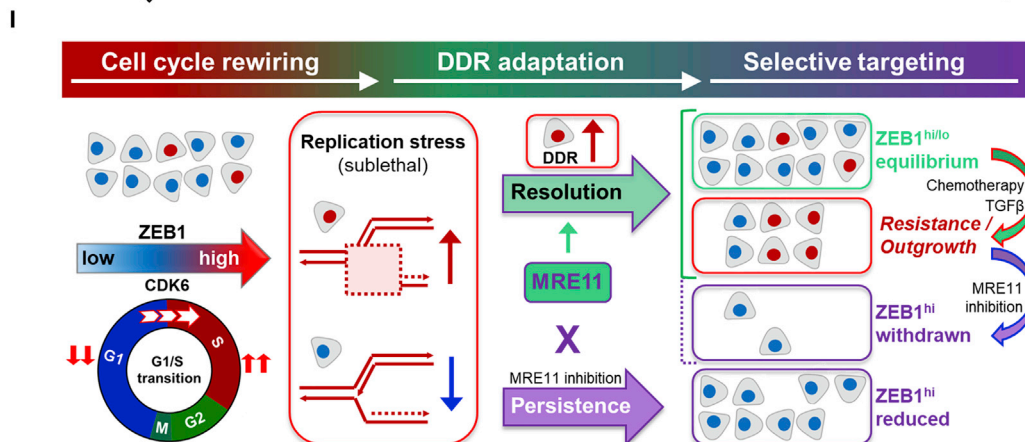
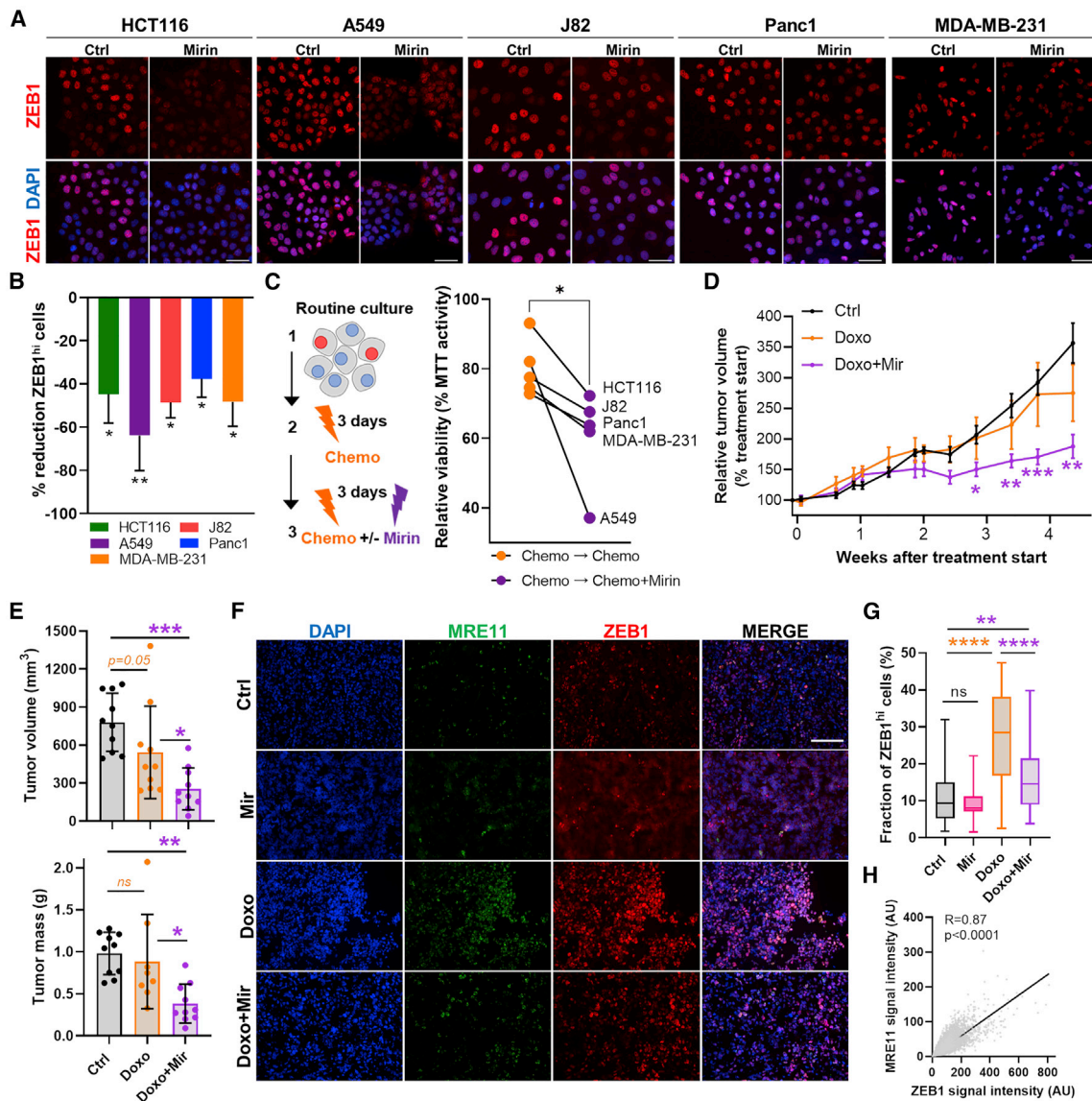
(G and H) HiMAC of ZEB1 with representative images after the indicated treatments (G). Red arrowheads indicate ZEB1<sup>hi</sup> cells and blue ones ZEB1<sup>lo</sup> cells. Scale bar, 40  $\mu$ m. Scatterplot in (H) depicts the distribution of total ZEB1 IF intensities, color coded as to ZEB1<sup>lo</sup> (blue) and ZEB1<sup>hi</sup> cells, among which ZEB1<sup>hi++</sup> (dark red) represent the top 20% of ZEB1<sup>hi</sup> cells and ZEB1<sup>hi+</sup> (light red) the remaining 80%. The bar graph shows the mean reduction of the indicated ZEB1<sup>hi</sup> cells after mirin treatment.

(I) Representative western blot of the indicated proteins in Ctrl-/TGF- $\beta$ -treated MCF10A cells  $\pm$  mirin and quantifications relative to  $\beta$ -actin.

(J) HiMAC of RAD51 foci in MCF10A treated as in (G).

(K) Cell-cycle profiles of Ctrl-/TGF- $\beta$ -treated MCF10A cells  $\pm$  mirin.

Data are depicted as the mean  $\pm$  SEM of n = 3 independent experiments (H, bottom panel, and K) or the means  $\pm$  SEM of >1,000 cells (B and C),  $\geq$  300 cells (E, F, and J), or >800 cells (H, top panel) per group of n  $\geq$  3 (B, C, E, and J) or n = 2 (F) independent experiments. Indicators (\*/#) mark significance, as determined by Mann-Whitney tests (C, E, F, H, top panel, and J) comparing ZEB1<sup>lo</sup> with ZEB1<sup>hi</sup> (\*) or ZEB1<sup>lo/hi</sup> with Ctrl (#), in C) and by two-way ANOVA with Sidak's post-test (K) comparing ZEB1<sup>hi</sup> with ZEB1<sup>lo</sup> (\*) and TGF- $\beta$  + mirin with TGF- $\beta$  (#). \*p < 0.05, \*\*p < 0.01, \*\*\*p < 0.001, \*\*\*\*p < 0.0001.



(legend on next page)

developmental progenitors,<sup>57</sup> it was proposed to contribute to TGF- $\beta$ -induced growth arrest.<sup>58</sup> The EMT-TFs ZEB2 and Snail, which are both not enriched in ZEB1<sup>hi</sup> MDA-MB-231, were reported to block proliferation by repressing cyclin D1 and cyclin D2, respectively,<sup>59,60</sup> together reinforcing functional specificities of EMT-TFs.<sup>29</sup> Contrasting these studies, but in line with a report on release from G1 synchronization,<sup>61</sup> we established a cell-line-independent role of ZEB1 in promoting G1/S transition showing that ZEB1<sup>hi</sup> cells commit earlier to S phase. Integrating sc and bulk transcriptomes as well as ZEB1 ChIP-seq data<sup>31</sup> to pinpoint likely direct targets of ZEB1, we demonstrate ZEB1-dependent expression of CDK6 and that its activity is required for the accelerated S-phase entry and the ensuing replication stress in TGF- $\beta$ -induced ZEB1<sup>hi</sup> cells. Together with the recently reported stabilization of ZEB1 by CDK6 via USP51,<sup>62</sup> our data suggest a feedforward loop of CDK6 and ZEB1 to drive G1/S transition. Notably, CDK6 abundance in melanoma can be restrained by miR200a,<sup>63</sup> a well-established reciprocal ZEB1 target,<sup>36,39</sup> altogether highlighting the key role of ZEB1 in promoting CDK6-driven S-phase entry.

Accordingly, TGF- $\beta$ -induced ZEB1<sup>hi</sup> MCF10A cells failed to reduce initiation of DNA synthesis and overrode the known TGF- $\beta$ -associated growth arrest.<sup>48,54</sup> Thus, the Janus faces of TGF- $\beta$  may be linked to the ZEB1<sup>hi/lo</sup> states, expanding ZEB1's established role in TGF- $\beta$ -associated EMT and malignancy by coupling EMT to proliferation.<sup>28,36,54</sup> Consistently, ZEB1 is required for initiating the outgrowth of dormant metastatic cancer cells.<sup>64</sup> Reconciling with other reports,<sup>65,66</sup> we propose that ZEB1 counteracts senescence by promoting S-phase entry.

We showed that ZEB1<sup>hi</sup> cells exhibit higher endogenous replication stress, which delayed their S-phase progression. Both DDR defects and/or premature S-phase entry are known to cause DNA replication stress.<sup>6,7,51,52</sup> In our study, ZEB1<sup>hi</sup> cells responded normally to the well-established replication poison HU, and several molecules from different DDR branches, such as PARP1, MRE11, and DNA-PKCs (PRKDCs), were upregulated in scRNA-seq. Thus, we reason that safe handling of damaged replication forks is retained in ZEB1<sup>hi</sup> cells due to co-activation of the DDR. This is in agreement with the concept that ZEB1 supports genomic stability and faithful DNA repair

via promotion of anti-oxidant defenses,<sup>66</sup> repression of the mutagenic end-joining polymerase theta,<sup>67</sup> or involvement of ATM to activate HR for DSB repair.<sup>42,43</sup> In this regard, MDA-MB-231 ZEB1<sup>hi</sup> cells in our study did not express higher mRNA levels of ATM (or ATR) but harbored more endogenous recombination substrates (RAD51 foci) than ZEB1<sup>lo</sup> cells, supporting enhanced recombination. Altogether, we conclude that ZEB1-dependent replication stress is caused by pushing the cells prematurely into S phase and can only be tolerated by co-activation of the DDR in ZEB1<sup>hi</sup> cells.

One of the major DDR effectors is p53. It is established that wild-type p53 can inhibit EMT, tumor cell invasiveness, and, particularly, EMT-related stemness features, for instance by transcriptional induction of miRNA200c negatively regulating EMT-TFs<sup>68</sup> or MDM2-mediated degradation of the EMT-TF Slug.<sup>69</sup> Since EMT-TFs can likewise inhibit p53 and other tumor-suppressive programs, it appears that a sophisticated mutual inhibition of EMT and p53 is governing EMT commitment and tumor suppression versus malignancy.<sup>70,71</sup> Intriguingly, in our study, there was no apparent dependence of the ZEB1<sup>hi</sup> phenotype on p53 status across the various cell lines we used, i.e., MCF10A (p53 wild-type [WT]), HCT116 (p53WT), A549 (p53WT), J82 (p53 mutant [mut]), Panc1 (p53 mut), and MDA-MB-231 (p53 mut). We thus conclude that p53 status seems not to dramatically affect the role of ZEB1 promoting S-phase entry triggering sub-lethal DNA replication stress. We reason that this might be due to the low intensity of stress induced, as exceeding the stress level by MRE11 inhibition indeed activated the G2/M checkpoint in MCF10A cells. In concert with reports that high ZEB1 expression does not correlate with p53 mutations in patients with cancer and that ZEB1 high expression is associated with genomic stability, at least in breast cancer,<sup>66</sup> it seems to us that ZEB1 high expression does not exert a selection pressure on p53 mutation. This, however, warrants further experimental proof.

We revealed correlated expression of ZEB1 and the MRN-complex member MRE11 in various cell lines as well as in TGF- $\beta$ -treated MCF10A cells and a selective dependency of ZEB1<sup>hi</sup> cells on MRE11 activity. Thus, our study not only introduced ZEB1 as an important fine-tuner of cell-cycle progression and

### Figure 6. Reducing ZEB1<sup>hi</sup> cells by MRE11 inhibition improves chemotherapy

- (A) Representative ZEB1 IF images after 72 h mirin treatment. Scale bar, 40  $\mu$ m.
- (B) Quantification of ZEB1<sup>hi</sup> cells from (A) relative to Ctrl treatment.
- (C) Cell viability measurement in cell lines treated with chemotherapy (chemo) and mirin as indicated in the scheme on the left. Cell viability relative to standard chemo (please refer to Figure S6C) is shown.
- (D) Relative longitudinal growth of subcutaneous MDA-MB-231 tumors intermittently treated with vehicles (Ctrl), doxorubicin (Doxo) alone, or Doxo plus mirin (Doxo + Mir) relative to tumor volume at treatment start (0 weeks).
- (E) Endpoint measurements of tumor volume (top) and tumor mass (bottom).
- (F–H) IF staining of ZEB1 and MRE11 of cryopreserved tumor sections (F) (tumors from D and E and Figures S6H–S6J) and quantifications showing fraction of ZEB1<sup>hi</sup> cells (G) and correlation of ZEB1 and MRE11 with Pearson's R and p value in individual cells from Ctrl-treated tumors (H). Scale bar: 100  $\mu$ m.
- Data are depicted as the means  $\pm$  SEM of  $n \geq 3$  independent experiments (B), the means of  $n \geq 3$  independent experiments (C), or the means of  $n \geq 9$  tumors  $\pm$ SEM (D),  $\pm$ SD (E), and minimum to maximum (Min-to-Max) plots of at least 14 fields of view derived from  $n \geq 9$  tumors (G). Asterisks (\*) mark significance as determined by Student's t test comparing chemo with respective Ctrl (B); paired t test comparing chemo with chemo + mirin (C); two-way ANOVA with Tukey's post-test comparing Ctrl versus Dox + mirin (D); one-way ANOVA with Holm-Sidak post-test as indicated (E), and Welch ANOVA (G). \* $p < 0.05$ , \*\* $p < 0.01$ , \*\*\* $p < 0.001$ , \*\*\*\* $p < 0.0001$ .
- (I) Model. Cell populations display heterogeneity in ZEB1 expression levels ranging from low (lo) to high (hi). ZEB1<sup>hi</sup> rewires cell cycling by promoting G1/S transition via CDK6, causing moderate endogenous DNA replication stress in ZEB1<sup>hi</sup> cells. This leads to an upregulation of DDR factors such as MRE11, allowing homeostasis of ZEB1<sup>hi/lo</sup> cells under normal conditions and ZEB1<sup>hi</sup> enrichment in response to TGF- $\beta$  or genotoxic chemotherapy. As MRE11 inhibition withdraws chemoresistant, but MRE11-dependent, ZEB1<sup>hi</sup> cells from the bulk population, it increases chemosensitivity.

DDR but also exposed a weak spot of chemoresistant ZEB1<sup>hi</sup> cells that is linked to S-phase DDR rewiring. As a proof of concept, we showed that the MRE11 inhibitor mirin chemosensitizes different cancer cells in concentrations that only reduced the ZEB1<sup>hi</sup> sub-population. Importantly, low-dose mirin co-treatment following Doxo pulses partially blocked the enrichment of resistant ZEB1<sup>hi</sup> cells by Doxo and sensitized MDA-MB-231 tumors in a xenograft model, causing tumor stasis. Of note, MRE11 expression is associated with poor survival and chemoresponse in several cancer entities<sup>72–74</sup> and was shown to mitigate replication stress in different cell culture models.<sup>75,76</sup> However, despite promising results in cell culture studies, mirin has not yet progressed to the clinics,<sup>77,78</sup> perhaps partially due to high dosing for bulk tumor cell targeting, neglecting intercellular heterogeneity in drug sensitivity. MRE11 is a major player in ATM activation, resection of DSBs for HR, and of replication forks to prevent or resolve replication intermediates, which can be either essential or detrimental, and it can inhibit the new firing of origins.<sup>45,55,79,80</sup> We found alterations in ZEB1<sup>hi</sup> cells in these features, namely increased helicase loading, indicative of increased origin firing, higher DNA synthesis rates, and rise in recombination intermediates. As the remaining ZEB1<sup>hi</sup> cells after MRE11 inhibition by mirin accumulated RAD51 foci and trended to S-phase delay and G2/M arrest, but showed no further increase in DNA synthesis rates, we favor the scenario that ZEB1<sup>hi</sup> cells are dependent on the function of MRE11 in fork remodeling.

The cell-cycle and ensuing DDR rewiring unleashed by ZEB1 is dispensable for proliferation under normal conditions but is necessary for full ZEB1 induction by TGF- $\beta$  and beneficial under genotoxic stress. Shortening of G1 phase causing moderate DNA replication stress is a known feature of stemness<sup>4,51,81,82</sup> that compromises chemotherapies by increasing replisome assemblies in S phase and hyper-activating the DDR.<sup>17,21,83,84</sup> Chemoresistant ZEB1<sup>hi</sup> cells are equipped with these armaments against genotoxic stress, and we propose that ZEB1 initiates the underlying cascade by enforcing S-phase entry via its likely target CDK6. Collectively, ZEB1-driven tuning of the cell cycle consequentially co-activating the DDR is a facet of ZEB1-related plasticity that aids well-known stemness and resistance features.<sup>26–28,38,42–44,66</sup> This provides a selection advantage for the ZEB1<sup>hi</sup> sub-population of cancer cells under stresses like TGF- $\beta$  exposure and chemotherapy, while imposing a translationally relevant selective weak spot, as we exemplified here by MRE11 inhibition. Targeting replication stress responses for cancer therapy has been proposed before.<sup>1,3,5,10,11,21,85</sup> Our study thus revealed the prospect of specifically targeting ZEB1-driven DDR adaptations, which often preclude successful cancer therapy.

### Limitations of the study

Our study exposes a targetable interplay of ZEB1 and the DDR. We show that by accelerated S-phase entry and subsequent mild replication stress, ZEB1<sup>hi</sup> cells exhibit an MRE11-engaging co-adaptation of the DDR, resulting in a survival benefit upon genotoxic stress. This comes with the cost of a co-dependence of ZEB1<sup>hi</sup> expressing cells on MRE11 *in vitro* and *in vivo*. However, we found that MRE11 inhibition or loss by siRNA-mediated knockdown only partially reduces ZEB1<sup>hi</sup> expressing cells, most evidently

observed after chemotherapy *in vivo*. Therefore, the DDR in ZEB1<sup>hi</sup> cells is most likely adapted on multiple levels, particularly in response to genotoxic stress. This extensive investigation of DDR plasticity was beyond the scope of our pioneering work but, for translational purposes, needs to be dissected in detail.

Mechanistically, we focused on CDK6 as driver of G1/S transition in ZEB1<sup>hi</sup> cells as it appeared to be a likely direct target of ZEB1 and was most consistently co-regulated with experimentally modulated ZEB1 expression. However, it is important to appreciate that our study does not rule out the possibility that other cell-cycle regulators participate in complex regulatory circuits to govern ZEB1-engaging transitions between cell-cycle phases. It also remains to be explored whether the ZEB1 status is interconvertible, switching from ZEB1<sup>lo</sup> to ZEB1<sup>hi</sup>, and vice versa, perhaps depending on environmental cues or stresses, as this would probably contribute to cellular plasticity. Mirin in combination with chemotherapy indeed showed promising effects on tumor growth leading to tumor stasis in immune-compromised mice. To our knowledge, though, the lack of clinically approved MRE11 inhibitors to date impede direct translation of our findings to cancer therapy. In this respect, our study fosters the idea of targeting the translationally relevant intersection of EMT and the DDR.

### STAR★METHODS

Detailed methods are provided in the online version of this paper and include the following:

- KEY RESOURCES TABLE
- RESOURCE AVAILABILITY
  - Lead contact
  - Materials availability
  - Data and code availability
- EXPERIMENTAL MODEL AND SUBJECT DETAILS
  - Mice
  - Cell lines
- METHOD DETAILS
  - Drug treatments
  - Cell viability assays
  - Generation of plasmids
  - Transfection
  - RNA extraction and RT-qPCR
  - Western blot analysis
  - Sorting of PIP-FUCCI cells
  - EdU labeling
  - Immunofluorescence and image acquisition
  - HiMAC
  - Cell cycle length measurement
  - Subcutaneous tumors and chemotherapy
  - Immunohistochemistry
  - Single-cell RNA sequencing and analysis
  - Analysis of public ZEB1 ChIP-seq data
- QUANTIFICATION AND STATISTICAL ANALYSIS

### SUPPLEMENTAL INFORMATION

Supplemental information can be found online at <https://doi.org/10.1016/j.celrep.2022.111819>.

## ACKNOWLEDGMENTS

We are grateful for Eva Bauer, Britta Schlund, and Friederike Gräbner for excellent technical assistance in the laboratory. We thank Uwe Appelt and Markus Mroz for excellent fluorescence-activated cell sorting (FACS) support. This work was supported by grants to S.B. and H.S. as well as F.B.E. from the Wilhelm Sander-Stiftung (2020.039.1; 2019.143.1); to T.B., S.B., M.P.S., and F.B.E. from the German Research Foundation (FOR2438/P04; TRR305/A03, A04, B07, and the Priority Programme SPP 2084, EN 453/13-1); and to M.P.S. from the European Union's Horizon 2020 research and innovation program under the Marie Skłodowska-Curie grant agreement no. 861196 (PRECODE).

## AUTHOR CONTRIBUTIONS

Conceptualization, H.S., S.B., and T.B.; methodology and validation, H.S., J.K., P.G., M.P.S., P.C., and T.K.; software, H.S., J.K., P.G., R.v.R., N.F., and V.R.; formal analysis, H.S., J.K., R.v.R., P.G., M.V., N.F., Y.H., and V.R.; investigation, H.S., J.K., I.A., M.K., K.F., M.M., M.H., and A.G.; resources, M.V., M.E., A.H., Y.H., N.F., R.v.R., F.M., and F.B.E.; writing – original draft, H.S. and J.K.; writing – review & editing, H.S., J.K., T.K., S.B., T.B., and M.P.S.; supervision, H.S., T.B., and S.B.; funding acquisition, H.S., S.B., T.B., and M.P.S.

## DECLARATION OF INTERESTS

The authors declare no competing interests.

Received: May 13, 2022

Revised: October 14, 2022

Accepted: November 22, 2022

Published: December 13, 2022

## REFERENCES

- Manic, G., Sistigu, A., Corradi, F., Musella, M., De Maria, R., and Vitale, I. (2018). Replication stress response in cancer stem cells as a target for chemotherapy. *Semin. Cancer Biol.* 53, 31–41. <https://doi.org/10.1016/j.semcancer.2018.08.003>.
- Vitale, I., Manic, G., De Maria, R., Kroemer, G., and Galluzzi, L. (2017). DNA damage in stem cells. *Mol. Cell* 66, 306–319. <https://doi.org/10.1016/j.molcel.2017.04.006>.
- Curtin, N.J. (2012). DNA repair dysregulation from cancer driver to therapeutic target. *Nat. Rev. Cancer* 12, 801–817. <https://doi.org/10.1038/nrc3399>.
- McGrail, D.J., Lin, C.C.J., Dai, H., Mo, W., Li, Y., Stephan, C., Davies, P., Lu, Z., Mills, G.B., Lee, J.S., and Lin, S.Y. (2018). Defective replication stress response is inherently linked to the cancer stem cell phenotype. *Cell Rep.* 23, 2095–2106. <https://doi.org/10.1016/j.celrep.2018.04.068>.
- Dreyer, S.B., Upstill-Goddard, R., Paulus-Hock, V., Paris, C., Lampraki, E.M., Dray, E., Serrels, B., Caligiuri, G., Rebus, S., Plenker, D., et al. (2021). Targeting DNA damage response and replication stress in pancreatic cancer. *Gastroenterology* 160, 362–377.e13. <https://doi.org/10.1053/j.gastro.2020.09.043>.
- Berti, M., Cortez, D., and Lopes, M. (2020). The plasticity of DNA replication forks in response to clinically relevant genotoxic stress. *Nat. Rev. Mol. Cell Biol.* 21, 633–651. <https://doi.org/10.1038/s41580-020-0257-5>.
- Kotsantis, P., Petermann, E., and Boulton, S.J. (2018). Mechanisms of oncogene-induced replication stress: jigsaw falling into place. *Cancer Discov.* 8, 537–555. <https://doi.org/10.1158/2159-8290.CD-17-1461>.
- Farmer, H., McCabe, N., Lord, C.J., Tutt, A.N.J., Johnson, D.A., Richardson, T.B., Santarosa, M., Dillon, K.J., Hickson, I., Knights, C., et al. (2005). Targeting the DNA repair defect in BRCA mutant cells as a therapeutic strategy. *Nature* 434, 917–921. <https://doi.org/10.1038/nature03445>.
- Bryant, H.E., Schultz, N., Thomas, H.D., Parker, K.M., Flower, D., Lopez, E., Kyle, S., Meuth, M., Curtin, N.J., and Helleday, T. (2005). Specific killing of BRCA2-deficient tumours with inhibitors of poly(ADP-ribose) polymerase. *Nature* 434, 913–917. <https://doi.org/10.1038/nature03443>.
- Gravells, P., Grant, E., Smith, K.M., James, D.I., and Bryant, H.E. (2017). Specific killing of DNA damage-response deficient cells with inhibitors of poly(ADP-ribose) glycohydrolase. *DNA Repair* 52, 81–91. <https://doi.org/10.1016/j.dnarep.2017.02.010>.
- Bukhari, A.B., Lewis, C.W., Pearce, J.J., Luong, D., Chan, G.K., and Gampfer, A.M. (2019). Inhibiting Wee1 and ATR kinases produces tumor-selective synthetic lethality and suppresses metastasis. *J. Clin. Invest.* 129, 1329–1344. <https://doi.org/10.1172/JCI122622>.
- Huang, A., Garraway, L.A., Ashworth, A., and Weber, B. (2020). Synthetic lethality as an engine for cancer drug target discovery. *Nat. Rev. Drug Discov.* 19, 23–38. <https://doi.org/10.1038/s41573-019-0046-z>.
- Sanjiv, K., Hagenkort, A., Calderón-Montaño, J.M., Koolmeister, T., Reaper, P.M., Mortusewicz, O., Jacques, S.A., Kuiper, R.V., Schultz, N., Scobie, M., et al. (2016). Cancer-specific synthetic lethality between ATR and CHK1 kinase activities. *Cell Rep.* 14, 298–309. <https://doi.org/10.1016/j.celrep.2015.12.032>.
- Housman, G., Byler, S., Heerboth, S., Lapinska, K., Longacre, M., Snyder, N., and Sarkar, S. (2014). Drug resistance in cancer: an overview. *Cancers* 6, 1769–1792. <https://doi.org/10.3390/cancers6031769>.
- Marusyk, A., Janiszewska, M., and Polyak, K. (2020). Intratumor heterogeneity: the rosetta stone of therapy resistance. *Cancer Cell* 37, 471–484. <https://doi.org/10.1016/j.ccell.2020.03.007>.
- Dagogo-Jack, I., and Shaw, A.T. (2018). Tumour heterogeneity and resistance to cancer therapies. *Nat. Rev. Clin. Oncol.* 15, 81–94. <https://doi.org/10.1038/nrclinonc.2017.166>.
- Carruthers, R.D., Ahmed, S.U., Ramachandran, S., Strathdee, K., Kurian, K.M., Hedley, A., Gomez-Roman, N., Kalna, G., Neilson, M., Gilmour, L., et al. (2018). Replication stress drives constitutive activation of the DNA damage response and radioresistance in glioblastoma stem-like cells. *Cancer Res.* 78, 5060–5071. <https://doi.org/10.1158/0008-5472.CAN-18-0569>.
- Bao, S., Wu, Q., McLendon, R.E., Hao, Y., Shi, Q., Hjelmeland, A.B., Dewhirst, M.W., Bigner, D.D., and Rich, J.N. (2006). Glioma stem cells promote radioresistance by preferential activation of the DNA damage response. *Nature* 444, 756–760. <https://doi.org/10.1038/nature05236>.
- Yin, H., and Glass, J. (2011). The phenotypic radiation resistance of CD44+/CD24(-or low) breast cancer cells is mediated through the enhanced activation of ATM signaling. *PLoS One* 6, e24080. <https://doi.org/10.1371/journal.pone.0024080>.
- Desai, A., Webb, B., and Gerson, S.L. (2014). CD133+ cells contribute to radioresistance via altered regulation of DNA repair genes in human lung cancer cells. *Radiother. Oncol.* 110, 538–545. <https://doi.org/10.1016/j.radonc.2013.10.040>.
- Manic, G., Musella, M., Corradi, F., Sistigu, A., Vitale, S., Soliman Abdel Rehim, S., Mattiello, L., Malacaria, E., Galassi, C., Signore, M., et al. (2021). Control of replication stress and mitosis in colorectal cancer stem cells through the interplay of PARP1, MRE11 and RAD51. *Cell Death Differ.* 28, 2060–2082. <https://doi.org/10.1038/s41418-020-00733-4>.
- Ihle, M., Biber, S., Schroeder, I.S., Blattner, C., Deniz, M., Damia, G., Gottifredi, V., and Wiesmüller, L. (2021). Impact of the interplay between stemness features, p53 and pol iota on replication pathway choices. *Nucleic Acids Res.* 49, 7457–7475. <https://doi.org/10.1093/nar/gkab526>.
- Mani, S.A., Guo, W., Liao, M.J., Eaton, E.N., Ayyanan, A., Zhou, A.Y., Brooks, M., Reinhard, F., Zhang, C.C., Shipitsin, M., et al. (2008). The epithelial-mesenchymal transition generates cells with properties of stem cells. *Cell* 133, 704–715. <https://doi.org/10.1016/j.cell.2008.03.027>.
- Morel, A.P., Lièvre, M., Thomas, C., Hinkal, G., Ansieau, S., and Puisieux, A. (2008). Generation of breast cancer stem cells through epithelial-mesenchymal transition. *PLoS One* 3, e2888. <https://doi.org/10.1371/journal.pone.0002888>.

25. Chaffer, C.L., Marjanovic, N.D., Lee, T., Bell, G., Kleer, C.G., Reinhardt, F., D'Alessio, A.C., Young, R.A., and Weinberg, R.A. (2013). Poised chromatin at the ZEB1 promoter enables breast cancer cell plasticity and enhances tumorigenicity. *Cell* 154, 61–74. <https://doi.org/10.1016/j.cell.2013.06.005>.
26. Shimono, Y., Zabala, M., Cho, R.W., Lobo, N., Dalerba, P., Qian, D., Diehn, M., Liu, H., Panula, S.P., Chiao, E., et al. (2009). Downregulation of miRNA-200c links breast cancer stem cells with normal stem cells. *Cell* 138, 592–603. <https://doi.org/10.1016/j.cell.2009.07.011>.
27. Wellner, U., Schubert, J., Burk, U.C., Schmalhofer, O., Zhu, F., Sonntag, A., Waldvogel, B., Vannier, C., Darling, D., zur Hausen, A., et al. (2009). The EMT-activator ZEB1 promotes tumorigenicity by repressing stemness-inhibiting microRNAs. *Nat. Cell Biol.* 11, 1487–1495. <https://doi.org/10.1038/ncb1998>.
28. Krebs, A.M., Mitschke, J., Lasierra Losada, M., Schmalhofer, O., Boerries, M., Busch, H., Boettcher, M., Mougiakakos, D., Reichardt, W., Bronsert, P., et al. (2017). The EMT-activator Zeb1 is a key factor for cell plasticity and promotes metastasis in pancreatic cancer. *Nat. Cell Biol.* 19, 518–529. <https://doi.org/10.1038/ncb3513>.
29. Stemmler, M.P., Eccles, R.L., Brabletz, S., and Brabletz, T. (2019). Non-redundant functions of EMT transcription factors. *Nat. Cell Biol.* 21, 102–112. <https://doi.org/10.1038/s41556-018-0196-y>.
30. Bronsert, P., Kohler, I., Timme, S., Kiefer, S., Werner, M., Schilling, O., Vashist, Y., Makowiec, F., Brabletz, T., Hopt, U.T., et al. (2014). Prognostic significance of Zinc finger E-box binding homeobox 1 (ZEB1) expression in cancer cells and cancer-associated fibroblasts in pancreatic head cancer. *Surgery* 156, 97–108. <https://doi.org/10.1016/j.surg.2014.02.018>.
31. Feldker, N., Ferrazzi, F., Schuhwerk, H., Widholz, S.A., Guenther, K., Frisch, I., Jakob, K., Kleemann, J., Riegel, D., Bönnich, U., et al. (2020). Genome-wide cooperation of EMT transcription factor ZEB1 with YAP and AP-1 in breast cancer. *EMBO J.* 39, e103209. <https://doi.org/10.15252/embj.2019103209>.
32. Liu, Y., Lu, X., Huang, L., Wang, W., Jiang, G., Dean, K.C., Clem, B., Telang, S., Jenson, A.B., Cuatrecasas, M., et al. (2014). Different thresholds of ZEB1 are required for Ras-mediated tumour initiation and metastasis. *Nat. Commun.* 5, 5660. <https://doi.org/10.1038/ncomms6660>.
33. Siebzehnrubl, F.A., Silver, D.J., Tugertimur, B., Deleyrolle, L.P., Siebzehnrubl, D., Sarkisian, M.R., Devers, K.G., Yachnis, A.T., Kupper, M.D., Neal, D., et al. (2013). The ZEB1 pathway links glioblastoma initiation, invasion and chemoresistance. *EMBO Mol. Med.* 5, 1196–1212. <https://doi.org/10.1002/emmm.201302827>.
34. Ruh, M., Stemmler, M.P., Frisch, I., Fuchs, K., van Roey, R., Kleemann, J., Roas, M., Schuhwerk, H., Eccles, R.L., Agaimy, A., et al. (2021). The EMT transcription factor ZEB1 blocks osteoblastic differentiation in bone development and osteosarcoma. *J. Pathol.* 254, 199–211. <https://doi.org/10.1002/path.5659>.
35. Shibue, T., and Weinberg, R.A. (2017). EMT, CSCs, and drug resistance: the mechanistic link and clinical implications. *Nat. Rev. Clin. Oncol.* 14, 611–629. <https://doi.org/10.1038/nrclinonc.2017.44>.
36. Brabletz, S., Schuhwerk, H., Brabletz, T., and Stemmler, M.P. (2021). Dynamic EMT: a multi-tool for tumor progression. *EMBO J.* 40, e108647. <https://doi.org/10.15252/embj.2021108647>.
37. Thiery, J.P., Acloque, H., Huang, R.Y.J., and Nieto, M.A. (2009). Epithelial-mesenchymal transitions in development and disease. *Cell* 139, 871–890. <https://doi.org/10.1016/j.cell.2009.11.007>.
38. Meidhof, S., Brabletz, S., Lehmann, W., Preca, B.T., Mock, K., Ruh, M., Schüller, J., Berthold, M., Weber, A., Burk, U., et al. (2015). ZEB1-associated drug resistance in cancer cells is reversed by the class I HDAC inhibitor mocetinostat. *EMBO Mol. Med.* 7, 831–847. <https://doi.org/10.15252/emmm.201404396>.
39. Caramel, J., Ligier, M., and Puisieux, A. (2018). Pleiotropic roles for ZEB1 in cancer. *Cancer Res.* 78, 30–35. <https://doi.org/10.1158/0008-5472.CAN-17-2476>.
40. Long, L., Xiang, H., Liu, J., Zhang, Z., and Sun, L. (2019). ZEB1 mediates doxorubicin (Dox) resistance and mesenchymal characteristics of hepatocarcinoma cells. *Exp. Mol. Pathol.* 106, 116–122. <https://doi.org/10.1016/j.yexmp.2019.01.001>.
41. Zou, J., Liu, L., Wang, Q., Yin, F., Yang, Z., Zhang, W., and Li, L. (2017). Down-regulation of miR-429 contributes to the development of drug resistance in epithelial ovarian cancer by targeting ZEB1. *Am. J. Transl. Res.* 9, 1357–1368.
42. Zhang, P., Wei, Y., Wang, L., Debeb, B.G., Yuan, Y., Zhang, J., Yuan, J., Wang, M., Chen, D., Sun, Y., et al. (2014). ATM-mediated stabilization of ZEB1 promotes DNA damage response and radioresistance through CHK1. *Nat. Cell Biol.* 16, 864–875. <https://doi.org/10.1038/ncb3013>.
43. Zhang, X., Zhang, Z., Zhang, Q., Zhang, Q., Sun, P., Xiang, R., Ren, G., and Yang, S. (2018). ZEB1 confers chemotherapeutic resistance to breast cancer by activating ATM. *Cell Death Dis.* 9, 57. <https://doi.org/10.1038/s41419-017-0087-3>.
44. Yang, J., Antin, P., Bex, G., Blanpain, C., Brabletz, T., Bronner, M., Campbell, K., Cano, A., Casanova, J., Christofori, G., et al. (2020). Guidelines and definitions for research on epithelial-mesenchymal transition. *Nat. Rev. Mol. Cell Biol.* 21, 341–352. <https://doi.org/10.1038/s41580-020-0237-9>.
45. Bruhn, C., Zhou, Z.W., Ai, H., and Wang, Z.Q. (2014). The essential function of the MRN complex in the resolution of endogenous replication intermediates. *Cell Rep.* 6, 182–195. <https://doi.org/10.1016/j.celrep.2013.12.018>.
46. Bruhn, C., Kroll, T., and Wang, Z.Q. (2014). Systematic characterization of cell cycle phase-dependent protein dynamics and pathway activities by high-content microscopy-assisted cell cycle phenotyping. *Dev. Reprod. Biol.* 12, 255–265. <https://doi.org/10.1016/j.gpb.2014.10.004>.
47. Lehmann, W., Mossmann, D., Kleemann, J., Mock, K., Meisinger, C., Brummer, T., Herr, R., Brabletz, S., Stemmler, M.P., and Brabletz, T. (2016). ZEB1 turns into a transcriptional activator by interacting with YAP1 in aggressive cancer types. *Nat. Commun.* 7, 10498. <https://doi.org/10.1038/ncomms10498>.
48. Mukherjee, P., Winter, S.L., and Alexandrow, M.G. (2010). Cell cycle arrest by transforming growth factor beta1 near G1/S is mediated by acute abrogation of prereplication complex activation involving an Rb-MCM interaction. *Mol. Cell Biol.* 30, 845–856. <https://doi.org/10.1128/MCB.01152-09>.
49. Zeman, M.K., and Cimprich, K.A. (2014). Causes and consequences of replication stress. *Nat. Cell Biol.* 16, 2–9. <https://doi.org/10.1038/ncb2897>.
50. Schuhwerk, H., Bruhn, C., Siniuk, K., Min, W., Erener, S., Grigaravicius, P., Krüger, A., Ferrari, E., Zübel, T., Lazaro, D., et al. (2017). Kinetics of poly(ADP-ribosylation), but not PARP1 itself, determines the cell fate in response to DNA damage in vitro and in vivo. *Nucleic Acids Res.* 45, 11174–11192. <https://doi.org/10.1093/nar/gkx717>.
51. Ahuja, A.K., Jodkowska, K., Teloni, F., Bizard, A.H., Zellweger, R., Herrador, R., Ortega, S., Hickson, I.D., Altmeyer, M., Mendez, J., and Lopes, M. (2016). A short G1 phase imposes constitutive replication stress and fork remodelling in mouse embryonic stem cells. *Nat. Commun.* 7, 10660. <https://doi.org/10.1038/ncomms10660>.
52. Macheret, M., and Halazonetis, T.D. (2018). Intragenic origins due to short G1 phases underlie oncogene-induced DNA replication stress. *Nature* 555, 112–116. <https://doi.org/10.1038/nature25507>.
53. Grant, G.D., Kedziora, K.M., Limas, J.C., Cook, J.G., and Purvis, J.E. (2018). Accurate delineation of cell cycle phase transitions in living cells with PIP-FUCCI. *Cell Cycle* 17, 2496–2516. <https://doi.org/10.1080/15384101.2018.1547001>.
54. Massagué, J. (2012). TGFbeta signalling in context. *Nat. Rev. Mol. Cell Biol.* 13, 616–630. <https://doi.org/10.1038/nrm3434>.
55. Doksan, Y., Bermejo, R., Fiorani, S., Haber, J.E., and Foiani, M. (2009). Replicon dynamics, dormant origin firing, and terminal fork integrity after double-strand break formation. *Cell* 137, 247–258. <https://doi.org/10.1016/j.cell.2009.02.016>.
56. Zierhut, C., and Diffley, J.F.X. (2008). Break dosage, cell cycle stage and DNA replication influence DNA double strand break response. *EMBO J.* 27, 1875–1885. <https://doi.org/10.1038/emboj.2008.111>.

57. Liu, Y., El-Naggar, S., Darling, D.S., Higashi, Y., and Dean, D.C. (2008). Zeb1 links epithelial-mesenchymal transition and cellular senescence. *Development* 135, 579–588. <https://doi.org/10.1242/dev.007047>.
58. Postigo, A.A. (2003). Opposing functions of ZEB proteins in the regulation of the TGFbeta/BMP signaling pathway. *EMBO J.* 22, 2443–2452. <https://doi.org/10.1093/emboj/cdg225>.
59. Vega, S., Morales, A.V., Ocaña, O.H., Valdés, F., Fabregat, I., and Nieto, M.A. (2004). Snail blocks the cell cycle and confers resistance to cell death. *Genes Dev.* 18, 1131–1143. <https://doi.org/10.1101/gad.294104>.
60. Mejlvang, J., Krijavetska, M., Vandewalle, C., Chernova, T., Sayan, A.E., Bex, G., Mellon, J.K., and Tulchinsky, E. (2007). Direct repression of cyclin D1 by SIP1 attenuates cell cycle progression in cells undergoing an epithelial mesenchymal transition. *Mol. Biol. Cell* 18, 4615–4624. <https://doi.org/10.1091/mbc.e07-05-0406>.
61. Wang, M., He, S.F., Liu, L.L., Sun, X.X., Yang, F., Ge, Q., Wong, W.K., and Meng, J.Y. (2017). Potential role of ZEB1 as a DNA repair regulator in colorectal cancer cells revealed by cancer-associated promoter profiling. *Oncol. Rep.* 38, 1941–1948. <https://doi.org/10.3892/or.2017.5888>.
62. Zhang, Z., Li, J., Ou, Y., Yang, G., Deng, K., Wang, Q., Wang, Z., Wang, W., Zhang, Q., Wang, H., et al. (2020). CDK4/6 inhibition blocks cancer metastasis through a USP51-ZEB1-dependent deubiquitination mechanism. *Signal Transduct. Target. Ther.* 5, 25. <https://doi.org/10.1038/s41392-020-0118-x>.
63. Bustos, M.A., Ono, S., Marzese, D.M., Oyama, T., Iida, Y., Cheung, G., Nelson, N., Hsu, S.C., Yu, Q., and Hoon, D.S.B. (2017). MiR-200a regulates CDK4/6 inhibitor effect by targeting CDK6 in metastatic melanoma. *J. Invest. Dermatol.* 137, 1955–1964. <https://doi.org/10.1016/j.jid.2017.03.039>.
64. De Cock, J.M., Shibue, T., Dongre, A., Keckesova, Z., Reinhardt, F., and Weinberg, R.A. (2016). Inflammation triggers zeb1-dependent escape from tumor latency. *Cancer Res.* 76, 6778–6784. <https://doi.org/10.1158/0008-5472.CAN-16-0608>.
65. de Barrios, O., Györfy, B., Fernández-Aceñero, M.J., Sánchez-Tilló, E., Sánchez-Moral, L., Siles, L., Esteve-Arenys, A., Roué, G., Casal, J.I., Darling, D.S., et al. (2017). ZEB1-induced tumorigenesis requires senescence inhibition via activation of DKK1/mutant p53/Mdm2/CtBP and repression of macroH2A1. *Gut* 66, 666–682. <https://doi.org/10.1136/gutjnl-2015-310838>.
66. Morel, A.P., Ginestier, C., Pommier, R.M., Cabaud, O., Ruiz, E., Wicinski, J., Devouassoux-Shisheboran, M., Combaret, V., Finetti, P., Chassot, C., et al. (2017). A stemness-related ZEB1-MSRB3 axis governs cellular plasticity and breast cancer genome stability. *Nat. Med.* 23, 568–578. <https://doi.org/10.1038/nm.4323>.
67. Prodhomme, M.K., Pommier, R.M., Franchet, C., Fauvet, F., Bergoglio, V., Brousset, P., Morel, A.P., Brunac, A.C., Devouassoux-Shisheboran, M., Petrilli, V., et al. (2021). EMT transcription factor ZEB1 represses the mutagenic POLtheta-mediated end-joining pathway in breast cancers. *Cancer Res.* 81, 1595–1606. <https://doi.org/10.1158/0008-5472.CAN-20-2626>.
68. Chang, C.J., Chao, C.H., Xia, W., Yang, J.Y., Xiong, Y., Li, C.W., Yu, W.H., Rehman, S.K., Hsu, J.L., Lee, H.H., et al. (2011). p53 regulates epithelial-mesenchymal transition and stem cell properties through modulating miRNAs. *Nat. Cell Biol.* 13, 317–323. <https://doi.org/10.1038/ncb2173>.
69. Wang, S.P., Wang, W.L., Chang, Y.L., Wu, C.T., Chao, Y.C., Kao, S.H., Yuan, A., Lin, C.W., Yang, S.C., Chan, W.K., et al. (2009). p53 controls cancer cell invasion by inducing the MDM2-mediated degradation of Slug. *Nat. Cell Biol.* 11, 694–704. <https://doi.org/10.1038/ncb1875>.
70. Semenov, O., Daks, A., Fedorova, O., Shuvalov, O., and Barlev, N.A. (2022). Opposing roles of wild-type and mutant p53 in the process of epithelial to mesenchymal transition. *Front. Mol. Biosci.* 9, 928399. <https://doi.org/10.3389/fmolb.2022.928399>.
71. Puisieux, A., Brabletz, T., and Caramel, J. (2014). Oncogenic roles of EMT-inducing transcription factors. *Nat. Cell Biol.* 16, 488–494. <https://doi.org/10.1038/ncb2976>.
72. Altan, B., Yokobori, T., Ide, M., Bai, T., Yanoma, T., Kimura, A., Kogure, N., Suzuki, M., Bao, P., Mochiki, E., et al. (2016). High expression of MRE11-RAD50-NBS1 is associated with poor prognosis and chemoresistance in gastric cancer. *Anticancer Res.* 36, 5237–5247. <https://doi.org/10.21873/anticancerres.11094>.
73. Wang, J., Xu, W.H., Wei, Y., Zhu, Y., Qin, X.J., Zhang, H.L., and Ye, D.W. (2019). Elevated MRE11 expression associated with progression and poor outcome in prostate cancer. *J. Cancer* 10, 4333–4340. <https://doi.org/10.7150/jca.31454>.
74. Yuan, S.S.F., Hou, M.F., Hsieh, Y.C., Huang, C.Y., Lee, Y.C., Chen, Y.J., and Lo, S. (2012). Role of MRE11 in cell proliferation, tumor invasion, and DNA repair in breast cancer. *J. Natl. Cancer Inst.* 104, 1485–1502. <https://doi.org/10.1093/jnci/djs355>.
75. Spehalski, E., Capper, K.M., Smith, C.J., Morgan, M.J., Dinkelmann, M., Buis, J., Sekiguchi, J.M., and Ferguson, D.O. (2017). MRE11 promotes tumorigenesis by facilitating resistance to oncogene-induced replication stress. *Cancer Res.* 77, 5327–5338. <https://doi.org/10.1158/0008-5472.CAN-17-1355>.
76. Petroni, M., Sardina, F., Infante, P., Bartolazzi, A., Locatelli, E., Fabretti, F., Di Giulio, S., Capalbo, C., Cardinali, B., Coppa, A., et al. (2018). MRE11 inhibition highlights a replication stress-dependent vulnerability of MYCN-driven tumors. *Cell Death Dis.* 9, 895. <https://doi.org/10.1038/s41419-018-0924-z>.
77. Velic, D., Couturier, A.M., Ferreira, M.T., Rodrigue, A., Poirier, G.G., Fleury, F., and Masson, J.Y. (2015). DNA damage signalling and repair inhibitors: the long-sought-after Achilles' heel of cancer. *Biomolecules* 5, 3204–3259. <https://doi.org/10.3390/biom5043204>.
78. Wang, Y.Y., Hung, A.C., Lo, S., Hsieh, Y.C., and Yuan, S.S.F. (2021). MRE11 as a molecular signature and therapeutic target for cancer treatment with radiotherapy. *Cancer Lett.* 514, 1–11. <https://doi.org/10.1016/j.canlet.2021.05.013>.
79. Ying, S., Hamdy, F.C., and Helleday, T. (2012). Mre11-dependent degradation of stalled DNA replication forks is prevented by BRCA2 and PARP1. *Cancer Res.* 72, 2814–2821. <https://doi.org/10.1158/0008-5472.CAN-11-3417>.
80. Olson, E., Nievera, C.J., Liu, E., Lee, A.Y.L., Chen, L., and Wu, X. (2007). The Mre11 complex mediates the S-phase checkpoint through an interaction with replication protein A. *Mol. Cell Biol.* 27, 6053–6067. <https://doi.org/10.1128/MCB.00532-07>.
81. Coronado, D., Godet, M., Bourillot, P.Y., Taponnier, Y., Bernat, A., Petit, M., Afanassieff, M., Markossian, S., Malashicheva, A., Iacone, R., et al. (2013). A short G1 phase is an intrinsic determinant of naive embryonic stem cell pluripotency. *Stem Cell Res.* 10, 118–131. <https://doi.org/10.1016/j.scr.2012.10.004>.
82. Matson, J.P., Dumitru, R., Coryell, P., Baxley, R.M., Chen, W., Twaroski, K., Webber, B.R., Tolar, J., Bielskiy, A.K., Purvis, J.E., and Cook, J.G. (2017). Rapid DNA replication origin licensing protects stem cell pluripotency. *Elife* 6, e30473. <https://doi.org/10.7554/eLife.30473>.
83. Ge, X.Q., Jackson, D.A., and Blow, J.J. (2007). Dormant origins licensed by excess Mcm2-7 are required for human cells to survive replicative stress. *Genes Dev.* 21, 3331–3341. <https://doi.org/10.1101/gad.457807>.
84. Ibarra, A., Schwob, E., and Méndez, J. (2008). Excess MCM proteins protect human cells from replicative stress by licensing backup origins of replication. *Proc. Natl. Acad. Sci. USA* 105, 8956–8961. <https://doi.org/10.1073/pnas.0803978105>.
85. O'Connor, M.J. (2015). Targeting the DNA damage response in cancer. *Mol. Cell* 60, 547–560. <https://doi.org/10.1016/j.molcel.2015.10.040>.
86. Spaderna, S., Schmalhofer, O., Wahlbuhl, M., Dimmler, A., Bauer, K., Sultan, A., Hlubek, F., Jung, A., Strand, D., Eger, A., et al. (2008). The transcriptional repressor ZEB1 promotes metastasis and loss of cell polarity in cancer. *Cancer Res.* 68, 537–544. <https://doi.org/10.1158/0008-5472.CAN-07-5682>.
87. Kametsky, L., Jones, T.R., Fraser, A., Bray, M.A., Logan, D.J., Madden, K.L., Ljosa, V., Rueden, C., Eliceiri, K.W., and Carpenter, A.E. (2011).

- Improved structure, function and compatibility for CellProfiler: modular high-throughput image analysis software. *Bioinformatics* 27, 1179–1180. <https://doi.org/10.1093/bioinformatics/btr095>.
88. Oki, S., Ohta, T., Shioi, G., Hatanaka, H., Ogasawara, O., Okuda, Y., Kawaji, H., Nakaki, R., Sese, J., and Meno, C. (2018). ChIP-Atlas: a data-mining suite powered by full integration of public ChIP-seq data. *EMBO Rep.* 19, e46255. <https://doi.org/10.15252/embr.201846255>.
89. Gruber, R., Zhou, Z., Sukchev, M., Joerss, T., Frappart, P.O., and Wang, Z.Q. (2011). MCPH1 regulates the neuroprogenitor division mode by coupling the centrosomal cycle with mitotic entry through the Chk1-Cdc25 pathway. *Nat. Cell Biol.* 13, 1325–1334. <https://doi.org/10.1038/ncb2342>.
90. Nowakowski, R.S., Lewin, S.B., and Miller, M.W. (1989). Bromodeoxyuridine immunohistochemical determination of the lengths of the cell cycle and the DNA-synthetic phase for an anatomically defined population. *J. Neurocytol.* 18, 311–318. <https://doi.org/10.1007/bf01190834>.
91. Siddiqui, A., Vazakidou, M.E., Schwab, A., Napoli, F., Fernandez-Molina, C., Rapa, I., Stemmler, M.P., Volante, M., Brabletz, T., and Ceppi, P. (2017). Thymidylate synthase is functionally associated with ZEB1 and contributes to the epithelial-to-mesenchymal transition of cancer cells. *J. Pathol.* 242, 221–233. <https://doi.org/10.1002/path.4897>.
92. Muraro, M.J., Dharmadhikari, G., Grün, D., Groen, N., Dielen, T., Jansen, E., van Gurp, L., Engelse, M.A., Carlotti, F., de Koning, E.J.P., and van Oudenaarden, A. (2016). A single-cell transcriptome Atlas of the human pancreas. *Cell Syst.* 3, 385–394.e3. <https://doi.org/10.1016/j.cels.2016.09.002>.
93. Li, H., and Durbin, R. (2010). Fast and accurate long-read alignment with Burrows-Wheeler transform. *Bioinformatics* 26, 589–595. <https://doi.org/10.1093/bioinformatics/btp698>.
94. Lun, A.T.L., McCarthy, D.J., and Marioni, J.C. (2016). A step-by-step workflow for low-level analysis of single-cell RNA-seq data with Bioconductor. *F1000Research* 5, 2122. <https://doi.org/10.12688/f1000research.9501.2>.
95. McCarthy, D.J., Campbell, K.R., Lun, A.T.L., and Wills, Q.F. (2017). Scater: pre-processing, quality control, normalization and visualization of single-cell RNA-seq data in R. *Bioinformatics* 33, 1179–1186. <https://doi.org/10.1093/bioinformatics/btw777>.

## STAR★METHODS

### KEY RESOURCES TABLE

REAGENT or RESOURCE	SOURCE	IDENTIFIER
<b>Antibodies</b>		
Rabbit polyclonal anti-53BP1	Novus Biologicals	Cat#NB100-304; RRID: AB_10003037
Mouse monoclonal anti- $\alpha$ -Tubulin	Sigma	Cat#T6199; RRID: AB_477583
Mouse monoclonal anti- $\beta$ -Actin	Sigma	Cat#A5441; RRID: AB_476744
Rabbit polyclonal anti- $\beta$ -Tubulin	Cell Signaling	Cat#cs2146; RRID: AB_2210545
Mouse monoclonal anti- $\gamma$ H2AX	Merck	Cat#05-636-l; RRID: AB_2755003
Rabbit polyclonal anti- $\gamma$ H2AX	Cell Signaling	Cat#cs2577; RRID: AB_2118010
Mouse monoclonal anti- CTIP	Active Motif	Cat#61142
Mouse monoclonal anti- E-cadherin	BD Biosciences	Cat#610182; RRID: AB_397581
Mouse monoclonal anti- Ki67	Cell Signaling	Cat#cs9449; RRID: AB_2797703
Mouse monoclonal anti- MCM2	BD Biosciences	Cat#610700; RRID: AB_2141952
Mouse monoclonal anti- MRE11	Novus Biologicals	Cat#NB100-473; RRID: AB_10001780
Rabbit polyclonal anti- NBS1	Novus Biologicals	Cat#NB100-143; RRID: AB_10078050
Mouse monoclonal anti- N-cadherin	BD Biosciences	Cat#610920; RRID: AB_2077527
Rabbit monoclonal anti- pRPA	Abcam	Cat#ab109394; RRID: AB_10860648
Mouse monoclonal anti- RAD50	GeneTex	Cat#GTX70228; RRID: AB_372854
Rabbit polyclonal anti- RAD51	Sigma	Cat#PC130; RRID: AB_2238184
Rabbit monoclonal anti- Vimentin	Cell Signaling	Cat#cs5741; RRID: AB_10695459
Rabbit polyclonal anti- ZEB1	Sigma	Cat#HPA027524; RRID: AB_1844977
Mouse monoclonal anti- ZEB1	Sigma	Cat#AMAb90510; RRID: AB_2665569
Rabbit polyclonal anti- ZEB1	Novus biologicals	Cat#NBP1-05987; RRID: AB_1556166
Phalloidin-Alexa-488	Thermo Fisher	Cat#A12379
Alexa488 Goat anti-Mouse IgG (H + L)	Thermo Fisher	Cat#A32723; RRID:AB_2633275
Alexa488 Goat anti-Rabbit IgG (H + L)	Thermo Fisher	Cat#A11034; RRID:AB_2576217
Alexa555 Goat anti-Mouse IgG (H + L)	Thermo Fisher	Cat#A21422; RRID:AB_2535844
Alexa555 Goat anti-Rabbit IgG (H + L)	Thermo Fisher	Cat#A32732; RRID:AB_2633281
CF640R Anti-Rabbit IgG (H + L)	Sigma	Cat#SAB4600164
<b>Bacterial and virus strains</b>		
psPAX2 (lentiviral packaging plasmid)	Addgene	Cat#12260; RRID: Addgene_12260
pMD2.G (viral envelope expression cassette)	Addgene	Cat#12259;RRID: Addgene_12259
CMV:Blast-PIP-FUCCI (PIP-FUCCI containing plasmid)	Addgene	Cat##138715; RRID: Addgene_138715
<b>Biological samples</b>		
Mouse Tumor cryosections	This paper	N/A
<b>Chemicals, peptides, and recombinant proteins</b>		
TGF $\beta$ 1	Peptotech	Cat#100-21
Mitomycin	Sigma	Cat#M4287
Camptothecin	R&D	Cat#1100
Doxorubicin	Sigma	Cat#44583
Gemcitabine	Sigma	Cat#G6423
Cisplatin	Sigma	Cat#C2210000
Hydroxyurea	Sigma	Cat#H6527
Palbociclib	Selleckchem	Cat#PD-0332991
Mirin	R&D	Cat#3190

(Continued on next page)

<b>Continued</b>		
REAGENT or RESOURCE	SOURCE	IDENTIFIER
PFM39	Sigma	Cat#SML1839
Thiazolyl blue tetrazolium bromide	Sigma	Cat#M2128
Lipofectamine RNAiMAX	Thermo Fisher	Cat#13778
FuGENE HD transfection reagent	Promega	Cat#E2311
Matrigel	Corning	Cat#356231
<b>Critical commercial assays</b>		
Click-iT® EdU Alexa Fluor® 647 Imaging Kit	Thermo Fisher	Cat#C10340
<b>Deposited data</b>		
Raw and analyzed data (single cell RNA sequencing)	This paper	GEO: GSE217273
Code for ChIPseq analysis ( <a href="http://chip-atlas.org">chip-atlas.org</a> )	This paper	Zenodo: <a href="https://doi.org/10.5281/zenodo.7304459">https://doi.org/10.5281/zenodo.7304459</a>
Original western blot images	This paper	Mendeley Data: <a href="https://doi.org/10.17632/dx7bk7p849.1">https://doi.org/10.17632/dx7bk7p849.1</a>
<b>Experimental models: Cell lines</b>		
Human: MCF10A	ATCC	Cat# CRL-10317; RRID: CVCL_0598
Human: MDA-MB-231	ATCC	Cat# HTB-26; RRID: CVCL_0062
Human: A549	ATCC	Cat# CCL-185
Human: Panc1	ATCC	Cat# CRL-1469; RRID: CVCL_0480
Human: J82	ATCC	Cat# HTB-1; RRID: CVCL_0359
Human: HCT116	Regine Schneider-Stock, University Hospital Erlangen, Germany	N/A
MDA-MB-231 shGFP/shZEB1	Spaderna et al. <sup>86</sup>	N/A
Panc1 shGFP/shZEB1	Wellner et al. <sup>27</sup>	N/A
MCF10A iZEB1	Lehmann et al. <sup>47</sup>	N/A
Panc1 ishCtrl/ishZEB1	This paper	N/A
MDA-MB-231 PIP-FUCCI	This paper/Arwin Groenewoud, FAU Erlangen, Germany.	N/A
SW620 PIP-FUCCI	This paper/Arwin Groenewoud, FAU Erlangen, Germany	N/A
<b>Experimental models: Organisms/strains</b>		
Nod-Scid-gamma	Fabian Müller, University Hospital Erlangen, Germany	N/A
<b>Oligonucleotides</b>		
siRNA targeting sequence negative Ctrl #1	Ambion (silencer select)	Cat#4390844
siRNA targeting sequence negative Ctrl #2	Ambion (silencer select)	Cat#4390847
siRNA targeting sequence CDK6#1 5'-GUUUGUACAGAUUCGAUTT-3'	Ambion (silencer select)	Cat# 4390824 (s51)
siRNA targeting sequence CDK6#1 5'GCAGAAAUGUUUCGUAGAATT-3'	Ambion (silencer select)	Cat# 4390824 (s53)
siRNA targeting sequence MRE11 5'-GGAUUUUGUUCUAGCUAAUTT-3'	Ambion (silencer select)	Cat#AM16708 (s144071)
siRNA targeting sequence ZEB1#1 5'-GGUAGAUGUAAUGUAAUATT-3'	Ambion (silencer select)	Cat#4392420 (s229971)
siRNA targeting sequence ZEB1#1 5'-GGAAGAACGUGACAGCACATT-3'	Ambion (silencer select)	Cat#4392420 (s229970)
Primers for qPCR, see <a href="#">Table S2</a>	This paper	N/A
<b>Recombinant DNA</b>		
pCDNA3.1 (+)	Thermo Fisher	Cat#V79020

(Continued on next page)

**Continued**

REAGENT or RESOURCE	SOURCE	IDENTIFIER
Software and algorithms		
CellProfiler 2.1.0	Kamentsky et al. <sup>87</sup>	N/A
GraphPad Prism Version 9.0.0	GraphPad Software	RRID: SCR_002798
Leica Application Suite X software	Leica	N/A
hiMAC	Bruhn et al. <sup>46</sup>	N/A
ChIP-Atlas	Oki et al. <sup>88</sup>	N/A

**RESOURCE AVAILABILITY**

**Lead contact**

Further information and requests for resources and reagents should be directed to and will be fulfilled by the lead contact, Harald Schuhwerk ([harald.schuhwerk@fau.de](mailto:harald.schuhwerk@fau.de)).

**Materials availability**

This study did not generate new unique reagents.

**Data and code availability**

- sc RNA-seq data have been deposited at GEO and are publicly available as of the date of publication. For accession numbers see the [key resources table](#). Original western blot images have been deposited at Mendeley and are publicly available. DOIs are listed in the [key resources table](#).
- All original code has been deposited at Zenodo and is publicly available as of the date of publication. DOIs are listed in the [key resources table](#).
- Any additional information required to reanalyze the data reported in this paper is available from the [lead contact](#) upon request.

**EXPERIMENTAL MODEL AND SUBJECT DETAILS**

**Mice**

All mouse experiments were approved by the Committee on Ethics of Animal Experiments of the State of Bavaria (Regierung Unterfranken, Würzburg) and performed according to European Animal Welfare laws and guidelines. NOD.Cg-Prkdcscid Il2rgtm1Wjl/SzJ (Nod-Scid-gamma, NSG) were bred by and received from Fabian Müller (Department of Hematology/Oncology, University Hospital Erlangen). Mice (male and female) used for subcutaneous tumor cell implantation were 8-10 week old at treatment start.

**Cell lines**

All cell lines were cultured under standard conditions (37°C, 5% CO<sub>2</sub>) and routinely tested for absence of mycoplasma. MDA-MB-231, A549, Panc1, J82 and SW620 cells were cultured in DMEM high glucose (Thermo Fisher, 31966) and HCT116 in McCoy's 5A medium (Thermo Fisher, 26600) each supplemented with 10% fetal bovine serum (Thermo Fisher, 10500) and 1% penicillin/streptomycin (Thermo Fisher, 15140). For stably transduced MDA-MB-231 and Panc1 shGFP and shZEB1 cell lines,<sup>27,86</sup> cell culture medium was additionally supplemented with 1 µg/mL puromycin (Sigma, P8833). Panc1 Dox-inducible knockdown clones for ZEB1 (ishZEB1) or non-silencing control (ishCtrl) were generated as described previously.<sup>47</sup> Briefly, the pTRIPZ\_ishZEB1 plasmid was generated by cloning of the shRNAmir cassette of pGIPZ ZEB1 (V3LHS\_356187, Open Biosystems) into the pTRIPZ vector backbone using XhoI and MluI. pTRIPZ Inducible Lentiviral Non-silencing shRNA Control (Open Biosystems) was used for generation of the Panc1 control cell line. ishPanc1 cells were selected using 3 µg/mL puromycin and knockdown was induced by adding 1 µg/mL Doxycycline (Dox) (Sigma, D3447) every other day for the indicated time. MCF10A cells were cultured in DMEM/F12 (Thermo Fisher Scientific, 31331) supplemented with 5% horse serum (Thermo Fisher Scientific, 16050), 20 ng/mL EGF (Peprotech, 100-15), 0.5 µg/mL hydrocortisone (Sigma, H0888), 0.1 µg/mL cholera toxin (Sigma, C8052), 10 µg/mL insulin (Sigma I9278) and 10 mM HEPES (Thermo Fisher Scientific, 15630). For TGFβ treatment MCF10A medium was supplemented daily with 5 ng/mL TGFβ1 (Peprotech, 100-21) for 10 days. Ectopic ZEB1 overexpression was induced in MCF10A iZEB1 cells<sup>47</sup> by adding 1 µg/mL Dox every other day for the indicated time. Control cells were treated with the final concentration of the corresponding solvent control (500 nM citric acid for TGFβ and 0.002% DMSO for Dox). For generation of PIP-Fucci cell lines, lentiviral particles were generated by transfecting a 10cm Petri dish of 70% confluent HEK293T cells with psPAX2 (lentiviral packaging plasmid), pMD2.G (viral envelope expression cassette) and pipFUCCI containing plasmid (CMV:Blast-PIP-FUCCI) with respective concentrations 0.72 pmol; 1.3 pmol; 1.64pmol. LipoD293 (25µL) was used to ensure high levels of transfection. Lentiviral particles were harvested after 72 h, clarified by centrifugation (5000 g, 5 min) and purified by passage through a 0.22 µm low protein binding filter (Millipore). MDA-MB-231 and

SW620 cells were transduced with 5-fold diluted lentiviral particles, incubating 24 h in the presence of 10  $\mu\text{g}/\text{mL}$  polybrene (Sigma, TR-1003). Transduced cells were selected with Blasticidin (1.25, 2.5 and 5  $\mu\text{g}/\text{mL}$ ) for two weeks until a stable cell line was obtained.

## METHOD DETAILS

### Drug treatments

To determine effects on ZEB1<sup>hi/lo</sup> population, TGF $\beta$ -treated MCF10A cells received either 60 nM Mitomycin C (MMC) for 24 h or 1  $\mu\text{M}$  Doxorubicin (Doxo) or 500 nM Camptothecin (CPT) for 30 min. Analysis was carried out 24 h or 48 h after release in drug-free but TGF $\beta$  containing medium, respectively. For analysis of ZEB1<sup>hi/lo</sup> distribution in cancer cells, they were treated for 72 h with sub-lethal cell line specific concentrations (MDA-MB-231 1 nM Doxo, Panc1 10 nM Gemcitabine (Gem), A549 1  $\mu\text{M}$  Cisplatin (CddP), J82 100 nM MMC, HCT116 1 nM CPT). To induce S-phase stress, MDA-MB-231, HCT116 and Ctrl-/TGF $\beta$ -treated MCF10A cells were incubated for 30 min with 2 mM Hydroxyurea followed either by direct fixation or allowing 3 h of recovery in drug free medium. Palbociclib (Palbo, Selleckchem, PD-0332991) was added to TGF $\beta$ -treated MCF10A cells for 24h (0.5  $\mu\text{M}$ ). Mirin treatment (R&D, 3190) was performed daily in parallel with TGF $\beta$  treatment in MCF10A cells (20  $\mu\text{M}$ ) or for 72 h in MDA-MB-231, A549, Panc1, J82, HCT116 (10  $\mu\text{M}$ ).

### Cell viability assays

For chemotherapy and Mirin combination treatment, cells were pre-treated with drugs for 3 days (HCT116 + 10 nM CPT, A549 + 10  $\mu\text{M}$  CddP, J82 + 100 nM MMC, Panc1 + 100  $\mu\text{M}$  Gem, MDA-MB-231 + 100 nM Doxo). Pre-treated cells were then seeded in quadruplicates in 96-well plates and either cultured for another 3 days in routine cell culture medium (standard Chemo), continuously with the respective drugs (Chemo  $\rightarrow$  Chemo) or with the respective drugs plus 10  $\mu\text{M}$  Mirin or PFM39 (Chemo  $\rightarrow$  Chemo + Mirin/ PFM39). For chemotherapy and MRE11 knockdown combination, pre-treated cells (3 days) were cultured for another 3 days with the respective chemotherapy plus either 10 nM Ctrl or MRE11 siRNA. MCF10A cells were seeded in quadruplicates in 96-well plates, pre-treated with 60 nM MMC for 24 h and then cultured for another 48 h with 60 nM MMC plus 10 nM Ctrl or MRE11 siRNA or 10  $\mu\text{M}$  MRE11 inhibitor PFM39. Cell viability was assessed using 5 mg/mL thiazolyl blue tetrazolium bromide (MTT, Sigma, M2128) according to the manufacturer's instructions and relative cell viability was determined relative to solvent control treated cells.

### Generation of plasmids

mmZEB1-EGFP (C-terminal fusion of EGFP to full length mouse ZEB1) was a kind gift of Andreas Eger and cloned via BamHI into pCDNA3.1. The corresponding ctrl EGFP only was cloned via EcoRI into pCDNA3.1.

### Transfection

For transient knockdown, cells were transfected with siRNA (10 nM) 24 h after seeding, using Lipofectamine RNAiMAX transfection reagent (Thermo Fisher, 13778) according to the manufacturer's instructions. Cells were analyzed 48 h or 72 h after transfection as indicated in the figure legend. siRNAs were obtained from Ambion (Silencer Select siRNAs, sequences provided in [key resources table](#)).

For transient overexpression, cells were transfected with 500 ng pcDNA3.1-EGFP or pcDNA3.1-mmZEB1-EGFP 24 h after seeding using FuGENE HD transfection reagent (Promega, E2311) according to the manufacturer's protocol. Cells were analyzed 72 h after transfection.

### RNA extraction and RT-qPCR

Total RNA was isolated and reversely transcribed using the RNeasy Plus Mini Kit (Qiagen, 74136) and the RevertAid First Strand cDNA Synthesis Kit (Thermo Fisher Scientific, K1622) according to the manufacturer's instructions. cDNA was amplified in 384 well plates using gene specific primers, the Universal Probe Library (Roche, 04869877001) and the TaqMan Universal Master Mix (Thermo Fisher Scientific, 4440040) according to the manufacturer's protocol. Samples were run in triplicates in a LightCycler 480 (Roche) and normalized to  $\beta$ -Actin or HPRT1.

### Western blot analysis

For whole cell protein cells were lysed in ice-cold lysis buffer (150 mM NaCl, 50 mM Tris-HCl pH 8.0, 0.5% Na-Desoxycholate (w/v), 0.1% SDS (v/v), 1% NP40 (v/v), 1 mM PMSF, 1  $\times$  complete protease inhibitor cocktail (Roche, 04693132001), 1  $\times$  PhosStop (Roche, 4906837001). Protein concentration was determined using the BCA Protein Assay (Thermo Fisher Scientific, 23225) in flat-bottom 96well plates according to the manufacturer's instructions. Protein samples were separated by SDS-PAGE, followed by wet blot transfer onto nitrocellulose membrane (Roth, 4685.1). Primary antibodies were applied o/n at 4°C, secondary antibodies for 1h at RT. For protein detection Western Lightning Plus ECL solution (Perkin-Elmer, NEL105001EA) and the ChemiDoc MP Imaging System (Bio-Rad) were used. Relative protein quantification was performed with ImageJ.

### Sorting of PIP-FUCCI cells

PIP-FUCCI reporter expressing MDA-MB-231 and SW620 cells were sorted into G1-, S- and G2/M-phase according to mVenus (PIP) and mCherry (Geminin<sub>1-110</sub>) expression using a MoFlo XDP cell sorter (Beckman Coulter). Subsequently, sorted cell fractions were lysed in lysis buffer and prepared for western blotting as described above.

### EdU labeling

For pulse-labeling with EdU (Thermo Fisher, C10340), cells were cultured with 10  $\mu$ M EdU for 45 min before fixation with 4% PFA.

### Immunofluorescence and image acquisition

For Immunofluorescence (IF) labeling cells seeded onto sterile glass coverslips were fixed in 4% PFA, quenched and permeabilized in 0.2% Triton-X/ 100 mM Glycine/ PBS and blocked in 3% BSA/PBS at RT. Primary and secondary antibodies were diluted in blocking solution and incubated for 1 h or 45min, respectively, at RT in a humidified chamber protected from light. EdU click reaction was carried out using the Click-iT® EdU Alexa Fluor® 647 Imaging Kit according to the manufacturer's instructions. Nuclei were stained with DAPI (Sigma, D9542) before coverslips were mounted onto glass slides with Citifluor™ AF1 solution (EMS, 17970-100). To determine chromatin-bound proteins (MCM2, pRPA), cells were incubated with extraction buffer (25 mM HEPES pH 7.5, 50 mM NaCl, 1 mM EDTA, 3 mM MgCl<sub>2</sub>, 300 mM glucose, 0.5% Triton X-100) for 5 min at 4°C prior to fixation. Images were acquired using a Leica DM5500 B microscope. Representative images were processed using the Leica Application Suite X software.

For IF on tissue sections, cryopreserved tumors embedded in Tissue Tek O.C.T. compound (Sakura), were thawed and equilibrated to RT, fixed in 4% PFA for one minute before IF staining as described above using primary antibodies at 4°C over night, followed by washing in PBS and incubation with secondary antibodies. IF images were acquired as described above and analyzed on the single cell level in batch using Cell Profiler. The mean of the upper 10% of ZEB1 signal intensities of individual cells from the Ctrl-treated tumor sections was set as a threshold for calculation of the fraction of ZEB1<sup>hi</sup> cells in all conditions.

### HiMAC

High content microscopy-assisted cell cycle phenotyping (hiMAC) was performed as published previously.<sup>46</sup> Raw image files were subjected to batch analysis using Cell Profiler<sup>87</sup> running an automated pipeline<sup>46</sup> to identify nuclei and foci and to measure fluorescence signal intensities with minor adjustment for each IF staining. Based on the total fluorescence signal intensities of DAPI (DNA content) and EdU (DNA synthesis), the cell cycle status was derived for individual cells (2N, EdU<sup>-</sup> = G1-phase, EdU<sup>+</sup> = S-phase, 2N, EdU<sup>-</sup> = G2/M-phase). Where indicated, S-phase was further divided into early, mid and late S-phase depending on DNA content. To distinguish between ZEB1<sup>hi</sup> and ZEB1<sup>lo</sup> cells, a threshold for ZEB1 total signal intensities was set. For MDA-MB-231, Panc1, A549, J82 and HCT116 cells, ZEB1 threshold was set by the 90<sup>th</sup> percentile of ZEB1 intensity in each cell line (i.e highest 10% ZEB1 expression was classified as ZEB1<sup>hi</sup>, remaining 90% of the cells as ZEB1<sup>lo</sup>). To identify newly generated ZEB1<sup>hi</sup> cells upon ZEB1 upregulation by TGF $\beta$ , a more stringent threshold was applied in MCF10A cells, set at the 95<sup>th</sup> percentile of ZEB1 intensity in solvent control (Ctrl) treated cells. Due to low the ZEB1 expression in MCF10A Ctrl cells, the bulk population is shown instead of the systematic categorization into ZEB1<sup>hi/lo</sup>. For ectopic ZEB1 induction via doxycycline in MCF10A iZEB1 cells and transient (ZEB1)-GFP overexpression in cancer cells, the ZEB1 threshold was empirically determined using intensities of non-induced/ non-transfected cells on the same coverslip. ZEB1 thresholds were always set using the untreated/solvent control treated sample and then applied to the treated conditions to determine changes in the ZEB1<sup>hi/lo</sup> fractions. To account for the increasing DNA content during S- and G2/M-phase, a threshold correction factor (1.3 for S-phase, 1.7 for G2/M-phase) was applied in all models.

For determination of cycling cells, cells were labeled with 10  $\mu$ M EdU for 24 h prior to fixation, followed by ZEB1 and Ki67 staining and subsequent hiMAC. Ki67 intensity thresholds were determined empirically for biological replicates. Cycling cells were defined as Ki67 and EdU positive cells, non-cycling cells as negative for Ki67 and/or EdU.

### Cell cycle length measurement

Cumulative EdU labeling was performed (45 min up to 18 h) and the length of the cell cycle as well as the lengths of individual phases were calculated as described previously.<sup>89,90</sup> Briefly, the length from one S-phase to the next S-phase was determined as the time point when the entire growth fraction (GF) was labelled with EdU (=T<sub>GF</sub>). The length of one complete cell cycle (T<sub>C</sub>) was calculated using the equation  $T_C = T_{GF} / (1 - LI_0)$ , with LI<sub>0</sub> representing the percentage of EdU<sup>+</sup> cells at the first labeling time point (45 min). To estimate the average length of the individual phases the following formulas were applied: S-phase: T<sub>C</sub> · T<sub>GF</sub>, G1-phase: % of G1 cells at first labeling time point × T<sub>C</sub>, G2/M-phase: % of G2/M cells at first labeling time point × T<sub>C</sub>.

### Subcutaneous tumors and chemotherapy

For subcutaneous tumors, 1 × 10<sup>6</sup> MDA-MB-231 cells in a mixture of Matrigel (Corning; 356231) and PBS (ratio of 2:1) were injected subcutaneously into the flanks of immune-deficient NSG mice. Tumor growth was measured two to three times per week. Chemotherapy started when the tumor volume exceeded 500mm<sup>3</sup>, as follows. Two weekly doses of vehicle (PBS) or Doxorubicin (Sigma-Aldrich; 44583; 1 mg/kg in PBS) were administered by intraperitoneal injections, followed by continuous two subcutaneous injections of Mirin (0.025 mg/kg per tumor in 0.3% DMSO in PBS) or vehicle (0.3% DMSO in PBS) per week (without doxorubicin) and another Doxorubicin pulse in week 4. Mice were sacrificed after 5 weeks of therapy or, accordingly, after 3 weeks of Mirin/DMSO monotherapy.

### Immunohistochemistry

Immunohistochemistry for ZEB1 on human breast, pancreatic and bladder cancer samples was performed as previously described.<sup>47</sup> Samples were retrieved from local archives, and usage was approved by the Ethics Committee of the University of Erlangen-Nuremberg (no. 374-14 Bc). For ZEB1 IHC on human non-small-cell lung cancer refer to.<sup>91</sup>

### Single-cell RNA sequencing and analysis

MDA-MB-231 single cell transcriptomes were generated using a commercially available 384-well plate approach from Single Cell Discoveries (Utrecht, Netherlands). Briefly, routinely cultured MDA-MB-231 cells were collected by trypsinization, resuspended in PBS and spotted as viable single cells into 384-well capture plates containing 50 nL of barcoded primers and 10  $\mu$ L of mineral oil (Sigma Aldrich) using a MoFlo Astrios EQ 1 fluorescence activated cell sorter (Beckman Coulter). The plates were then briefly centrifuged at high speed and stored at  $-80^{\circ}\text{C}$  until shipping on dry ice and further processing at Single Cell Discoveries (SCD). Library preparation, sequencing and alignment was performed by SCD.<sup>92</sup> Briefly, after heat-lysis of the cells at  $65^{\circ}\text{C}$ , sequential barcoding, amplification and *in vitro* transcription was performed to generate a final cDNA library containing TruSeq small RNA primers (Illumina) for sequencing. Quality and quantity of the cDNA libraries was determined by Bioanalyzer before paired-end sequencing on an Illumina Nextseq<sup>TM</sup> 500. Paired-end reads were then aligned to the ensemble transcriptome (GRCh38) using BWA.<sup>93</sup> The corresponding transcript count table was generated using a custom-written script (<https://github.com/anna-alemany/transcriptomics/tree/master/mapandgo>). Downstream processing involving quality controls and filtering (with regards to UMIs, total genes and percentage of mitochondrial reads per cells), normalization, feature detection, dimensionality reduction, clustering and differential expression analysis between clusters or groups was performed using the in-built functions in within the packages Scran version 1.18.5<sup>94</sup> and Scater version 1.18.5.<sup>95</sup> In total, 568 MDA-MB-231 sc transcriptomes were generated and used for downstream analyses. For identifying differences in the gene expression profile in context of ZEB1, cells were grouped into 'ZEB1<sup>hi</sup>' and 'ZEB1<sup>lo</sup>' if the ZEB1 count in these cells were 'higher' or 'lower than equal to' a threshold expression count of 3 (the 3<sup>rd</sup> quartile ZEB1 expression value, see Figure S2C), respectively. Finally, functional enrichment analysis on significantly dysregulated genes (FDR<0.05) in 'ZEB1<sup>hi</sup>' cells was performed using Metascape (<https://metascape.org/>) or EnrichR (<https://maayanlab.cloud/Enrichr/>), as indicated.

For analyzing the sc transcriptomes of the lung cancer-brain metastasis PDX (sample LC-MBT-15; profile GSE69405 in GEO), the cells were categorized using the 3<sup>rd</sup> quartile as cutoff for 'ZEB1<sup>hi</sup>'. The gene set Hallmark 'G2M checkpoint' was then analyzed for enrichment with Signal2Noise ranking metric between ZEB1<sup>hi</sup> and 'ZEB1<sup>lo</sup> (below cutoff) cells.

### Analysis of public ZEB1 ChIP-seq data

ZEB1 ChIP-seq datasets (ChIP-Atlas,<sup>88</sup>) with a significance threshold greater than 5 ( $-10 \log_{10}[\text{Q-value}]$ ), MACS2, FDR Q < 0.00001) are included. Genomic coordinates of the promotor (distance  $\pm 1\text{kb}$  from transcription start site) in target gene lists were resolved using UCSC Genome Browser (NCBI RefSeq, hg38). Overlapping features of ZEB1 ChIP-seq datasets and target gene lists were detected using bedtools (v2.30.0).

Dataset	Cell type
SRX100456	GM12878
SRX190265	Hep G2
ERX3507564	MDA-MB-231 (1)
ERX3507565	MDA-MB-231 (2)
SRX2245437	MIA_Paca-2 (1)
SRX2245441	MIA_Paca-2 (2)
SRX2245442	MIA_Paca-2 (3)
ERX1930087	NCH421k
SRX3392333	NCI-H1975 (1)
SRX3392334	NCI-H1975 (2)
ERX1930086	Neural_Stem_Cells
SRX825399	PANC-1

### QUANTIFICATION AND STATISTICAL ANALYSIS

Statistical analyses were performed using GraphPad Prism and the applied statistical tests as well as the number of replicates (n) are specified in the relevant figure legends. p values < 0.05 were considered significant and are indicated in the figures. Data are presented as the mean  $\pm$  standard error of the mean (SEM) unless otherwise indicated in the relevant figure legends.